Substrate-dependent suppression of oxidative phosphorylation in the Frataxin-depleted heart

César Vásquez-Trincado[1], Monika Patel[1], Aishwarya Sivaramakrishnan[1], Carmen Bekeová[1], Lauren Anderson-Pullinger[1], Nadan Wang[2], Erin L. Seifert[1,*].

[1] MitoCare Center for Mitochondrial Imaging Research and Diagnostics, Department of Pathology, Anatomy and Cell Biology, Thomas Jefferson University, Philadelphia, PA, USA

[2] Center for Translational Medicine, Department of Pathology, Anatomy and Cell Biology, Thomas Jefferson University, Philadelphia, PA, USA

[*] Correspondence: Erin.Seifert@jefferson.edu

Running Title: Frataxin loss and selective oxphos suppression

ABSTRACT

Friedreich's ataxia is an inherited disorder caused by depletion of frataxin (FXN), a mitochondrial protein involved in iron-sulfur cluster biogenesis. Cardiac dysfunction is the main cause of death; pathogenesis remains poorly understood but is expected to be linked to an energy deficit. In mice with adult-onset FXN loss, bioenergetics analysis of heart mitochondria revealed a time- and substrate-dependent decrease in oxidative phosphorylation (oxphos). Oxphos was lower with substrates that depend on Complex I and II, but preserved for lipid substrates. This differential substrate vulnerability is consistent with the half-lives for mitochondrial proteins, and with the abundance of Fe-S clusters in proteins of different substrate oxidation pathways. Though cardiac contractility was preserved, likely due to sustained β-oxidation, a stress response was stimulated, characterized by activated mTORC1 and the p-eIF2α/ATF4 axis. Indeed, global protein translation was lower, which may account for a decrease in FXN-depleted hearts, and would help to lower ADP demand, which would be protective. This study exposes an unrecognized mechanism that maintains oxphos in the FXN-depleted heart. The stress response that nonetheless occurs suggests energy deficit-independent pathogenesis.

KEYWORDS

Frataxin; bioenergetics; β-oxidation; cardiac metabolism; mitochondrial disease; integrated stress response

INTRODUCTION

Friedreich's Ataxia (FRDA) is caused by an expansion repeat of GAA between exon 1 and 2 of the gene encoding Frataxin (FXN). This leads to depletion of FXN which is part of the protein machinery responsible for iron-sulfur (Fe-S) cluster biogenesis located in the mitochondrial matrix. It is accepted that FXN depletion below 30% of normal levels leads to pathology, the severity of which is generally correlated with GAA expansion length (Reetz, Dogan et al., 2015). FRDA is characterized by a fully penetrant ataxia, as well as other manifestations, such as cardiomyopathy, that are not fully penetrant (Kipps, Alexander et al., 2009, St John Sutton, Ky et al., 2014, Tsou, Paulsen et al., 2011).

Cardiac dysfunction is the main source of mortality in FRDA, accounting for 59% of deaths (Tsou et al., 2011). Yet, its pathogenesis, including its partial penetrance, is not well understood, though it might be assumed that a major energy deficit, caused by loss of oxidative phosphorylation capacity, is a driver of pathology. Energy deficit seems logical as a source of pathology since the heart has an incessant requirement for ATP which it gets from oxidative phosphorylation, and three of the electron transport chain complexes require Fe-S centers for electron transfer, as do other enzymes and related proteins within the mitochondrial matrix. Yet substrate oxidation pathways have not, to our knowledge, been studied in detail in cellular or animal models of FRDA.

An elegant time course study using the CKM (creatine kinase, muscle isoform) model of FXN loss points to the activation of the integrated stress response (ISR) as an event concurrent with or preceding an energy deficit in the heart (Huang, Sivagurunathan et al., 2013). The ISR involves phosphorylation of eIF2α (p- eIF2α) that leads to a decrease in global translation on the one hand, and, on the other hand, to an increase in translation of genes induced by the transcription factor ATF4 (Costa-Mattioli & Walter, 2020, Pakos-Zebrucka, Koryga et al., 2016). Induction of several genes can serve as a readout of the ISR, and this induction is observed in many models of other mitochondrial diseases (Bao, Ong et al., 2016, Dogan, Cerutti et al., 2018, Forsstrom, Jackson et al., 2019, Khan, Nikkanen et al., 2017, Nikkanen, Forsstrom et al., 2016, Quiros, Prado et al., 2017, Suomalainen, Elo et al., 2011). Considering other mitochondrial diseases, a small number of cell model-based studies reported a rise in p-eIF2α (Quiros et al., 2017), while the majority of mouse-based studies have focused on a rise in steady state mTORC1 signaling (Johnson, Yanos et al., 2013) (Civiletto, Dogan et al., 2018, Khan et al., 2017, Siegmund, Yang et al., 2017), as well as changes in associated pathways such as AMPK signaling (Dogan et al., 2018, Viscomi, Bottani et al., 2011) and autophagy (Civiletto et al., 2018). All these other pathways have been less studied in the heart of FRDA models including the CKM mouse. Yet, the CKM model features

cardiac hypertrophy (Huang et al., 2013, Seznec, Simon et al., 2004, Stram, Wagner et al., 2017, Wagner, Pride et al., 2012), which is not easily explained by elevated p-eIF2α and an ensuing decrease in global translation. Taken together, the mitochondrial disease literature suggests that multiple signaling pathways can be altered to potentially drive phenotypes. Thus, in any given model, it would be useful to broadly understand disrupted signaling. A broader understanding could expand the possible therapeutic targets and also reveal if disease heterogeneity needs to be considered in the context of FRDA treatments.

The CKM mouse model of FXN loss has been useful because it exhibits severe cardiac dysfunction (Huang et al., 2013, Martin, Abraham et al., 2017, Seznec et al., 2004); indeed it has been used to demonstrate the potential of gene replacement therapy in the heart (Belbellaa, Reutenauer et al., 2019, Perdomini, Belbellaa et al., 2014). Yet, this model features complete depletion of FXN from birth and thus might reflect a developmental response. Moreover, the model has a rapid time course, making it more challenging to disentangle causes from consequences of severe pathology. A recently developed model of adult-onset FXN depletion (Chandran, Gao et al., 2017) has several advantages for the study of the pathogenesis of cardiomyopathy in FRDA: the model avoids a developmental context, and has a wider window of time without overt major cardiac pathology. We used this model to investigate the progression of cardiac mitochondrial metabolism and nutrient and stress signaling changes with the goal of obtaining insight into the pathogenesis of FXN loss in the heart, specifically with regard to the impact on energy metabolism and how changes in energy metabolism might drive pathology.

RESULTS

Model of adult-onset doxycycline-induced FXN depletion

The genetic mouse model used here to deplete FXN is the same as that used by Chandran and colleagues (Chandran et al., 2017), however the doxycycline (Doxy) dosing regimen differed. Chandran supplied Doxy by intraperitoneal injection (5 mg/kg, with a 3-week span at 10 mg/kg) and the drinking water (2 mg/ml), whereas we supplied Doxy in the chow (200 p.p.m. throughout) to induce FXN depletion. Though both studies started the Doxy dosing at ~9 weeks of age, and the different Doxy dosing regimens yielded models with some similarities, there are important differences exist (see Discussion); thus we suggest that the models resulting from the two dosing regimens be considered as different models of FXN depletion.

After 8 weeks of Doxy feeding, FXN was barely detectable in the heart of TG mice, and the degree of protein knockdown was stable after that (Figure 1A). General phenotypic changes were evident from 12 weeks of Doxy diet. TG mice had a noticeable greying of the coat color, whereas WT mice showed no such changes. Moreover, TG mice started to die after ~16 weeks of Doxy feeding whereas no WT mice died (Figure 1B). TG mice also lost weight. During the first 12-14 weeks of Doxy diet, WT and TG body weights were comparable, but, after that, TG mice experienced a progressive weight loss (Figure 1C). Based on these findings, we focused our studies on two time points: 8-10 weeks of Doxy diet (soon after FXN protein depletion) and 17-20 weeks (some weight loss, some mortality).

Compensated heart function in FXN-depleted hearts

Cardiac hypertrophy is often a feature of the cardiomyopathy of FRDA (Tsou et al., 2011). Thus, we measured heart weight in both WT and TG mice at 17-20 weeks of Doxy feeding. Strikingly, heart weight/tibia length ratio (HW/TL) was lower in TG hearts (Figure 1D). Accordingly, we measured cardiac fiber size in WT and TG hearts from 17-20 weeks of Doxy diet and we found a tendency for smaller fiber size in FXN-depleted hearts (Figure 1E). To check if the decrease in heart size might be an intrinsic characteristic of TG mice, we measured heart weight in mice without Doxy feeding, and found no differences between WT and TG (Figure S1A). To evaluate cardiac function, we serially performed echocardiography. Over the course of Doxy feeding, fractional shortening (FS) was slightly greater in TG compared to WT mice (Figure 1F). Left ventricular inner diameter at end-diastole (LVIDd) and at end-systole (LVIDs), both parameters used to calculate FS, showed a continuous trend for smaller values in FXN-depleted hearts (Figure 1F). To assess cardiovascular function under physiological elevated workload, mice ran on a treadmill using an endurance protocol. WT and TG fed with Doxy for 8-10 and 17-20 weeks ran for a similar period time under the treadmill endurance protocol (Figure 1G). Additionally, blood lactate levels were measured as an indicator of glycolytic flux which might be higher if aerobic capacity is less, to compensate for the higher workload imposed by exercise. WT and TG mice (8-10 weeks and 17-20 weeks of Doxy diet) showed similar lactate levels before and after running (Figure 1H). Supporting normal cardiac function, Masson's trichrome staining was negative for collagen deposition in TG hearts (Figure 1I). Moreover, transcripts levels of *Myh6* (α-MHC) and *Myh7* (β-MHC), which respectively tend to decrease and increase in heart failure (Razeghi et al., 2001), where higher and lower respectively (Figure 1J), supporting the absence of cardiac hypertrophy. However, under FXN-depletion, the heart displayed abnormal electrical activity, as measured by ECG (Figure 1K). The abnormal rhythm was evident in TG mice starting

at 8 weeks of the Doxy diet and was characterized the absence of a J wave (interpreted as heterogeneity in early repolarization) (Boukens, Rivaud et al., 2014) and a longer QT interval (Figure 1K). There was also a clear decrease in heart rate in TG mice (Figure 1K). Altogether, these results indicate that TG cardiac contractility was not dysfunctional (despite an abnormal ECG), and this could support the increased workload of exercise without an abnormal rise in blood lactate levels.

Selective suppression of substrate oxidation in heart mitochondria from Tg mice

To understand if oxidative phosphorylation (oxphos) was compromised in FXN-depleted hearts, we performed bioenergetics analysis in isolated heart mitochondria from mice fed with Doxy for 8-10 and 17-20 weeks. Oxygen consumption rate (JO_2) was used to evaluate the oxidation of three sets of substrates: pyruvate (with malate), succinate (in presence of rotenone) and palmitoyl-L-carnitine (with malate) (Figure 2B, S2A). To oxidize these substrates, several Fe-S clusters-containing pathways are needed, and some of those pathways are common while others are substrate-specific (Figure 2A). Moreover, the pathways depend on different numbers of Fe-S cluster-containing proteins (Figure 2A); for example, oxidation of pyruvate relies on more Fe-S cluster-containing than does fatty acid-derived electron supply to Complex III via the electron transfer flavoprotein dehydrogenase (see Figure 2A). Thus, it was of interest to investigate each of these substrates. In heart from TG mice, there was a time-dependent decrease in maximal ADP- driven JO_2 and FCCP-stimulated JO_2 with the supply of pyruvate/malate (Figure 2B). Using succinate as a substrate, heart mitochondria from TG mice exhibited the same levels of JO_2 as mitochondria from WT mice, at 8-10 weeks of Doxy diet (Figure 2B). However, at 17-20 weeks of Doxy-feeding showed a significant decrease in maximal ADP- and FCCP-stimulated JO_2 (Figure 2B). In contrast, supply with palmitoyl-L-carnitine (PCarn)/malate induced similar levels of maximal ADP- and FCCP-stimulated JO_2 at the two time points (Figure 2B). We noted that maximal ADP-driven JO_2 with PCarn/malate in WT mitochondria was much lower than with pyruvate/malate, and therefore considered the possibility that the lack of decrease in PCarn-driven JO2 in TG mitochondria might reflect the fact that JO_2 was already low in WT mitochondria. To address this possibility, we used octanoyl-L-carnitine (Figure 2C) which, despite its shorter carbon chain length (C8:0), had higher max oxphos than palmitoyl-L-carnitine (C16:0), likely because more substrate can be used without causing uncoupling (Wojtczak & Schonfeld, 1993). Using octanoyl-L-carnitine, we obtained higher JO_2 values for WT mitochondria (Figure 2C), compared when PCarn/malate was a used as a substrate, although WT and TG maximal ADP-stimulated JO_2 were similar (Figure 2C). Unexpectedly, maximal oligomycin-insensitive JO_2 was

lower in TG heart mitochondria (Figure 2B and 2C), suggesting decreased proton leak. To further assess this in heart mitochondria from 17-week Doxy mice, we evaluated proton leak as a function of driving force (membrane potential, ΔΨm) by titrating octanoyl-L-carnitine with antimycin in the presence of oligomycin. Consistently, heart mitochondria from TG hearts exhibited less JO_2 at the same ΔΨm compared to WT mitochondria (Figure 2D), indicating lower proton leak in TG mitochondria oxidizing octanoyl-L-carnitine. Finally, Cytochrome c/Complex IV status was evaluated using TMPD/ascorbate as an electron donor; there were no significant differences between WT and TG heart mitochondria (Figure S2B). Altogether, these results suggest that not all Fe-S-containing pathways were equally affected by FXN loss; in particular, β-oxidation was preserved.

Defects in electron transport chain complex and supercomplex abundance and activity in TG heart mitochondria

To further interpret the bioenergetics data, immunoblotting of electron transport chain subunits and substrate oxidation enzymes was performed in heart mitochondria. For mice fed Doxy for 8-10 weeks, electron transport chain subunits were similar in WT and TG heart mitochondria, although some decrease in Cytochrome c was detected (Figure S3A). We checked if heart mitochondria from TG mice that were not fed with Doxy had lower Cytochrome c levels, and they did not (Figure S3B). For mice fed Doxy for 17-20 weeks, compared to WT, TG heart mitochondria exhibited small decreases, or a tendency for a small decrease, in several proteins, namely NDUFA9 (Complex I subunit), SDHB (Complex II, Fe-S-containing), and ETFDH (β-oxidation; Fe-S-containing), but no change in other proteins (SDHA (Complex II), UQCRC2 (Complex III), MTCO2 (Complex IV), ATP5A (ATP synthase) and ETFA (β-oxidation)) (Figure 3A).

Because electron transport chain subunits function in complexes, and some of these assemble into higher order complexes (supercomplexes: SC), we performed BN-PAGE to determine complex SC abundance and activity in heart mitochondria from mice fed Doxy for 17-20 weeks. The abundance of assembled Complex III, IV and V was similar between WT and TG heart mitochondria (Figure 3B). However, FXN-depleted mitochondria exhibited lower levels of assembled Complex I and II (Figure 3B). Abundance of SCs also was lower in TG heart mitochondria (Figure 3B). To have a better insight of the functionality of the complexes, we measured in-gel activity (IGA). TG heart mitochondria showed decreased Complex I (Figure 3C) and Complex II activity (Figure 3D, Figure S3C, S3D). In contrast Complex V activity, was similar between WT and TG heart mitochondria (Figure 3E).

To further investigate substrate oxidation within the mitochondrial matrix, we checked general indicators of the matrix environment, namely protein acetylation and 4-hydro-nonenal (4-HNE) oxidative modification of mitochondrial proteins. A generalized increased in protein acetylation of mitochondrial proteins from TG hearts was evident in TG mice fed Doxy for 17-20 weeks (Figure S3E); elevated acetylation on lysine residues indicates an imbalance in acetyl-CoA synthesis versus its metabolism or efflux, and was also evident in heart mitochondria from CKM mice (Martin et al., 2017, Stram et al., 2017, Wagner et al., 2012). On the other hand, there was no evidence for elevated 4-HNE protein adducts in mitochondria from TG hearts, (Figure S3F); thus, elevated lipid-induced oxidative modification was not greater in TG hearts.

Finally, to test for a metabolic switch that is usually present in cardiac hypertrophy or failure (Wende, Brahma et al., 2017), we evaluated mRNA levels of transporters and enzymes involved in glucose transport and metabolism (*Slc2a4*, *Hk2*, *Pfkfb1*) and fatty acid transport and metabolism (*Cd36*, *Cpt1b*, *Acadm*). There was no major difference between WT and TG hearts from 17-20 weeks of Doxy feeding (Figure 3F).

Altogether, these results further support that not all Fe-S cluster-containing pathways were equally affected by FXN depletion; specifically, among the electron transport chain complexes, Complex III activity appeared to be preserved.

Stress signaling and aberrant nutrient signaling in FXN-depleted hearts

Though heart function was normal/compensated in FXN-depleted mice, mitochondrial function, though likely adequate to meet ATP demand, was not normal. Thus, we wondered if TG hearts might exhibit alterations in signaling, namely mTORC1 signaling, that have been documented in models of other primary mitochondrial diseases (e.g., (Khan et al., 2017)). In the TG hearts from mice fed Doxy for 17-20 weeks, we detected a dysregulation of the mTORC1 pathway. Though, phosphorylation status of mTOR (Ser 2448) showed no difference between WT and TG hearts (Figure 4A, 4B), downstream components of this pathway were more activated in TG hearts (Figure 4A, 4C and 4D). FXN-depleted hearts exhibited higher levels of p-S6 (Figure 4A, 4C) and p-4EBP1 (Figure 4A, 4D). For p-P70-S6K, there was a trend for an increase in TG hearts (Figure S4A, S4B). Additionally, we evaluated the phosphorylation of eukaryotic translation initiation factor 2 alpha (eIF2α), the core event of activation of the integrated stress response (ISR) pathway

(Pakos-Zebrucka et al., 2016). We found in TG-hearts from 17-20 weeks of Doxy diet, substantially higher levels of phosphorylated eIF2α compared to WT hearts (Figure 4E).

To look for downstream manifestations of mTORC1/ISR activation, we measured levels of transcripts that are typically induced (e.g., (Forsstrom et al., 2019, Quiros et al., 2017)). At 8-10 weeks with Doxy diet, we found no differences between WT and TG hearts (Figure S4D). In contrast, TG hearts from mice fed Doxy for 17-20 weeks showed higher mRNA levels of one-carbon metabolism enzymes (Figure 4F, S4C), components of amino acid transport/metabolism (Figure 4H), *Fgf21* (Figure 4I) and, importantly *Atf4*, a key component in ISR transcriptional response (Figure 4G). There was no difference in *Atf2*, *Atf3* (Figure 4G), *Gdf15*, *Atf5* (Figure 4G), and also in the proteases *Clpp* and *Lonp1* (Figure 4J) that play a role in mitochondrial quality control. Additionally, MTHFD2 protein levels were significant elevated in TG hearts from mice of 17-20 weeks of Doxy diet (Figure 4K). Altogether, these results point to an activation of a stress response in FXN-depleted hearts that is frequently observed with primary mitochondrial dysfunction. This occurred despite preserved heart function and energy production in TG hearts.

Finally, because mTORC1 pathway and eIF2α activation involve changes in protein synthesis balance, we monitored global protein translation *in vivo*, using the SUnSET method (Schmidt, Clavarino et al., 2009). We detected a decrease in global protein synthesis in FXN-depleted hearts from mice after 17-20 weeks of Doxy diet (Figure 4L). In addition to protein synthesis, we evaluated protein degradation components. At 17-20 weeks of Doxy feeding, we found no differences in mRNA levels of E3 ubiquitin ligases, Atrogin1 (*Fbxo32*) and MuRF1 (*Trim63*), between WT and TG hearts (Figure S4E). Consistent with a lack of difference in degradation, the amount of polyubiquitinated proteins witth specific lysine (K) linkages (K48 and K63) were similar between WT and FXN-depleted hearts (Figures S4F and S4G).

Altogether, these results show decreased global protein synthesis in TG hearts (but not protein degradation), that could explain the reduced heart size under FXN depletion.

Insights into upstream regulators of eIF2α and mTORC1

We found increased levels of p-eIF2α in TG hearts from 17-20 weeks of Doxy diet, (Figure 4E), indicting induction of the ISR. ER stress can trigger the ISR (Pakos-Zebrucka et al., 2016). Thus, we evaluated phosphorylated levels of PERK, one of the upstream regulators of eIF2α, but found

no differences between WT and TG hearts (Figure 5A). Additionally, BIP/GRP78 levels, usually increased during ER stress, were unchanged (Figure S5A).

Evaluating mTORC1 regulators (Costa-Mattioli & Walter, 2020), we monitored the activation of AMPK and AKT, in FXN-depleted hearts. Because mTOR is negatively regulated by AMPK (Costa-Mattioli & Walter, 2020), we measured the phosphorylation status of this kinase and found a consistent decrease in p-AMPK in FXN-depleted (Figure 5B). We also checked the phosphorylation status of AKT kinase, a classical regulator of mTORC1, and found higher levels of p-AKT (Thr308 and Ser473) in TG-heart lysates (Figure 5C).

Increased levels of intracellular iron have been linked with activation of AKT (Varghese, James et al., 2018). We examined iron accumulation (ferric iron deposition) in WT and TG hearts from mice fed for 17-20 weeks on Doxy diet. We found positive staining only in TG hearts (Figure 5D, 5E). To put the iron deposition in TG hearts into the context of the iron homeostatic response, we measured iron metabolism regulators in heart lysates from mice fed Doxy for 17-20 weeks. We found elevated protein levels of FTH1 (Ferritin heavy chain) and Ferroportin and lower Transferrin receptor (*Tfrc*) mRNA levels in TG hearts (Figure 5F, 5G), consistent with an appropriate homeostatic response to elevated iron levels (Anderson, Shen et al., 2012).

Altogether, these findings provide insights into the upstream regulators of mTORC1 and eIF2α in FXN-depleted hearts, which are further discussed, below.

DISCUSSION

We undertook a detailed analysis of mitochondrial bioenergetics in FXN-depleted heart mitochondria, because this was generally lacking in models of FRDA, yet seemed important to do because several mitochondrial proteins, including subunits of the electron transport chain, depend on Fe-S clusters for proper function. Our analysis revealed some expected findings, such as some lowering of oxphos (using pyruvate and succinate as a substrates), but also unexpectedly revealed a preservation of oxphos from β-oxidation. These findings provide novel insights into mechanisms that could underlie the variability in the incidence and extent of cardiac pathology in individuals with FRDA. Also, they raise the possibility that cells with the flexibility to use fatty acids for oxphos, such as the heart, may be better able to maintain some oxphos despite substantial FXN depletion.

Elevated mTORC1 signaling reported in mouse models of other mitochondrial diseases (Johnson et al., 2013) (Civiletto et al., 2018, Khan et al., 2017, Siegmund et al., 2017) prompted us to further investigate nutrient and stress signaling in the heart of TG mice. We found evidence for an ISR, as was also found in the CKM mouse model of FRDA (Huang et al., 2013). But, mTORC1 signaling was also elevated in TG mice, and changes in other signaling pathways were evident. Further investigation into the possible impact of these alterations in signaling revealed lower global protein translation, which could explain the small hearts in FXN-depleted mice (Figure S6). Our data suggest that multiple changes in signaling can be present, with certain changes having a predominant influence on phenotypes.

The genetic mouse model used here is the same as that used by Chandran and colleagues (Chandran et al., 2017), with the exception of the Doxy dosing regimen (Chandran supplied Doxy by intraperitoneal injection and in drinking water). The time course and extent of FXN depletion from the heart, and also body weight loss, were similar in the two studies. However, differences are apparent in cardiac function and histology. Notably, while Chandran reported an abnormal ECG as we did, they also observed hypertrophy and collagen deposition indicating fibrosis after 24 wks of Doxy (Chandran et al., 2017). Cardiac hypertrophy and fibrosis, along with decreased ejection fraction, were also evident in the CKM model (Huang et al., 2013, Martin et al., 2017, Seznec et al., 2004, Stram et al., 2017, Wagner et al., 2012), as were markers of apoptosis (Huang et al., 2013). CKM mice have complete FXN depletion in the heart from birth, and it is unclear if developmental factors play a role in the early and severe cardiac pathology found in that model. The FXN-depleted mice in the present study showed no signs of fibrosis or hypertrophy and in fact had decreased heart weight and maintained (even increased) cardiac contractility. Maintained contractility might be related to the higher expression of α-MHC in TG hearts, since α-MHC is linked to higher contractile power compared to β-MHC isoform (Herron, Korte et al., 2001, Herron & McDonald, 2002). It is noteworthy that mortality of the mice used in the present study was lower than reported by Chandran (~25% by 16 weeks of Doxy, compared to ~50% reported by Chandran). Chandran tested several Doxy doses, and higher dose was associated with greater mortality. Thus, it is possible the Doxy dose used in the present study was lower than the lowest dose used by Chandran (and on which they reported phenotypes). Importantly, beyond the same genetic underpinnings, the models generated by Chandran and us differ in terms of cardiac effects and should thus be considered as different models of FXN depletion, at least in the context of the heart. We further suggest that both models are relevant given the variation in cardiac phenotypes seen in individuals with FRDA.

Sustained cardiac contractility and the absence of changes in transcript levels of glycolytic and β-oxidation enzymes, both of which often change when the heart is in energy crisis (Wende et al., 2017), suggest that cardiac energy production was sufficient in the FXN-depleted hearts. How is this possible? Though maximal oxphos was lower for some substrates, this maximal rate includes a reserve capacity that would allow for some compromise before ATP demand cannot be met. Thus, it is possible that the decrease in maximal oxphos largely reflected removal of a "buffer". However, isoproterenol challenge, that would use some of this reserve capacity, did not worsen heart function in TG mice (data not shown). While this could indicate that sufficient reserve capacity remained in the heart of TG mice, a more likely explanation for sustained energy production is the preservation of oxphos from fatty acid substrates, especially considering the heart normally generates much of its ATP from β-oxidation. Interestingly, mice with only half the normal complex I-driven oxphos in the heart, due to depletion of a complex I assembly factor, had, like TG mice, normal heart function including during dobutamine stimulation (Karamanlidis, Lee et al., 2013); it would be interesting to determine if β-oxidation is normal in that model. Oxphos from β-oxidation can bypass the TCA cycle, because electrons can enter Complex III from the acyl-CoA dehydrogenases, via ETF and ETFDH; this source of electrons could serve as a metabolic bypass in mitochondrial diseases that lower Complex I function. In the Tg mice, this metabolic bypass would allow for less reliance on the TCA cycle and Complex I. Greater oxphos efficiency, evidenced by lower proton leak-dependent respiration (Figure 2D), might also help to preserve β-oxidation.

We were surprised to find that substrate oxidation was not drastically decreased and was not uniformly affected by FXN loss. Though we could not find a direct reference to this phenomenon, a review of the literature on the effects of depletion of Fe-S cluster biogenesis components revealed some bias for greater suppression of Complex I and II over Complex III (Figure S7) (Crooks, Maio et al., 2018, Lim, Friemel et al., 2013, Navarro-Sastre, Tort et al., 2011, Rotig, de Lonlay et al., 1997), in line with our observations. Our study also indicates that the capacity for electron flow from β-oxidation into Complex III via the ETFDH (one Fe-S cluster) (see Figure 2A) is preserved. We discuss two mechanisms that might lead to a differential vulnerability of Fe-S cluster proteins to FXN depletion. First, a low rate of FXN-independent Fe-S cluster biogenesis can occur in hypoxia (Ast, Meisel et al., 2019). Low O_2 tension might be present in the matrix of heart mitochondria due to the incessant high rates of ATP synthesis; low partial pressure of O_2 in the coronary sinus is consistent with this possibility, and estimates of *in vivo* PO_2 of cardiac mitochondria indicate that ~a third of mitochondria have $PO_2 < 20$ mmHg, and 10% less than 10 mmHg (Mik, Ince et al., 2009). Thus, a low rate of Fe-S cluster biogenesis might occur in FXN-

depleted heart mitochondria, with some proteins, such as the ETFDH and Rieske protein of Complex III, having preferential access to new Fe-S clusters. Another possibility is differential rates of protein degradation. Among Fe-S cluster proteins in the heart, ETFDH has the longest half- life (~17 days) and SDHB the shortest (~9 days) (Fornasiero, Mandad et al., 2018), in line with our oxphos data. On the other hand, most Fe-S cluster-containing Complex I subunits and the Rieske protein had similar half-lives (~12 days) (Fornasiero et al., 2018). Our observations indicate preserved Complex III but lower Complex I activity. Possibly, protein half-life is prolonged when proteins are assembled into a complex, and more so for Complex III than for Complex I whose N module, which protrudes into the matrix, is susceptible to greater turnover (Szczepanowska, Senft et al., 2020). Yet, differential protein degradation might not fully explain our findings because protein levels of SDHB and Complex II in-gel activity, though decreased, were higher than might be expected given the relatively short half-life of Complex II subunits (Fornasiero et al., 2018). Thus, an additional mechanism, such as FXN-independent Fe-S cluster biogenesis, may account for the remarkable preservation of substantial ETC capacity in FXN-depleted hearts. It is also noteworthy that electron supply from acyl-CoA dehydrogenases to Complex III via ETFDH relies on fewer Fe-S clusters than does electron supply from pyruvate (see Figure 2A).

It is well documented in cell and mouse models that primary mitochondrial dysfunction is associated with upregulated transcripts induced by ATF4 (Bao et al., 2016, Dogan et al., 2018, Forsstrom et al., 2019, Khan et al., 2017, Nikkanen et al., 2016, Quiros et al., 2017, Tyynismaa, Carroll et al., 2010), including in the heart (Kuhl, Miranda et al., 2017). Elevated circulating FGF21 in humans with myopathy caused by mitochondrial DNA mutations suggests this is present also in humans (Suomalainen et al., 2011). Furthermore, elevated mTORC1 signaling has been detected in several mouse models of mitochondrial disease, and rapamycin treatment can prevent the aforementioned transcriptional response and lessen some pathological phenotypes (Civiletto et al., 2018, Johnson, Yanos et al., 2015, Johnson et al., 2013, Khan et al., 2017, Siegmund et al., 2017, Zheng, Boyer et al., 2016). Thus, although cardiac contractility and β-oxidation were normal in TG hearts, abnormalities in other mitochondrial functions, suggested by lower maximal oxphos for pyruvate and succinate, and higher lysine acetylation of mitochondrial proteins, prompted us to investigate mTORC1 signaling and levels of ATF4-induced transcripts in TG hearts. We found, after ~4.5 months of FXN loss, evidence for elevated mTORC1 signaling along with the induction of transcripts typically upregulated in mitochondrial disease. Elevated p-eIF2α was also detected, indicating the induction of the integrated stress response (ISR). Elevated p-eIF2α was also evident in the CKM model of FXN loss (mTORC1 signaling was not studied)

(Huang et al., 2013); this precedes obvious changes in cardiac function (Huang et al., 2013), but is roughly concurrent with the appearance of increased acetylation of mitochondrial proteins that indicate some disturbance of metabolic flux (Stram et al., 2017). Interestingly, mice with mtDNA mutations demonstrated a staged development of a stress response (Forsstrom et al., 2019) that did not appear well coupled to electron transport chain deficiency. In hearts from TG mice, ISR was not apparent at 10 weeks of FXN depletion, when there were no major changes in oxphos or protein acetylation, but some loss of Cytochrome c was observed. Thus, a threshold or type of mitochondrial dysfunction needs to be reached for the induction of the ISR or elevated mTORC1 signaling. However, a major energy deficit does not seem to be required for induction.

We sought insights into mechanisms that could activate mTORC1 signaling and elevate p-eIF2α. Elevated p-AMPK has been detected in several models of mitochondrial skeletal myopathy (Dogan et al., 2018, Viscomi et al., 2011), so we were surprised to find it decreased in TG hearts. Interestingly, hearts with greatly diminished β-oxidation (due to knockout of acyl-CoA synthase-1) also had lower p-AMPK (Ellis, Mentock et al., 2011). AMPK negatively regulates mTORC1 by phosphorylating and activating the mTORC1 inhibitor TSC2 (Liu & Sabatini, 2020); thus, lower AMPK activity would remove that source of inhibition of mTORC1. AKT can also phosphorylate, but this results in TSC2 activation (Liu & Sabatini, 2020). Thus, higher p-AKT levels in TG hearts could also lead to higher mTORC1 signaling. Elevated p-AKT could also explain lower p-AMPK, as shown in the heart (Kovacic, Soltys et al., 2003, Soltys, Kovacic et al., 2006), by phosphorylation of the AMPK-α1 subunit that prevents activating phosphorylation from upstream kinases (Hawley, Ross et al., 2014). Interestingly, elevated p-AKT has been linked to increased intracellular iron (Varghese et al., 2018). Regarding elevated p-eIF2α, ER stress is a trigger, and ER stress has been documented in mitochondrial myopathy (Pereira, Tadinada et al., 2017); but ER stress was not apparent in TG hearts. Recently, the kinase Heme Regulated Inhibitor (HRI) was shown to link mitochondrial dysfunction to increased p-eIF2α (Guo, Aviles et al., 2020). The canonical condition for HRI activation is heme depletion (Han, Yu et al., 2001). We did not evaluate HRI activation (phosphorylation) because, to our knowledge, reliable methods do not exist for mouse cells. However, Cytochrome c levels were decreased, consistent with heme depletion, and heme deficiency has been shown in several mammalian cells with FXN depletion (Schoenfeld, Napoli et al., 2005). Thus, it seems reasonable to suggest that HRI is the activating kinase of eIF2α in TG hearts.

Elevated mTORC1 signaling would predict hypertrophy of TG hearts (e.g. (Ellis et al., 2011)). Yet, TG hearts were smaller, suggesting that the effect of peIF2α to decrease global protein translation

overrode mTORC1 activation. Indeed, we found evidence for lower global protein translation in TG hearts. We also checked protein degradation but found no induction of atrogenes nor change in protein ubiquitination suggesting that degradation was not higher in TG hearts. The CKM model, in which FXN is lost from birth, also featured elevated p-eIF2α (Huang et al., 2013), though cardiac hypertrophy was also evident (Huang et al., 2013, Seznec et al., 2004, Stram et al., 2017). Unfortunately, mTORC1 signaling was not evaluated in CKM mice. It is possible that elevated p-eIF2α and mTORC1-dependent signaling coexist, but that the extent of hypertrophy depends on which pathway predominates.

Our study has several implications. First, it suggests that the variable penetrance of cardiac phenotypes in FRDA may be related to the multiplicity of changes in nutrient and stress signaling that can occur, the relative importance of which might differ among individuals, leading to variable phenotypes such as hypertrophy or lack thereof. Second, in relatively less affected patients, i.e. those with shorter repeat expansions and more FXN protein, oxphos might be maintained in part by the stability of some ETC complexes and other matrix proteins. Third, our study indicates that normal heart function and energy production can be misleading indicators that the FXN-depleted heart is normal, because we show that abnormalities, involving multiple nutrient and stress signaling pathways, can be present even when heart function and oxphos are adequate. Fourth, the impact of FXN depletion on substrate metabolism can be substrate-dependent, with relative preservation of β-oxidation; thus FXN-depleted cells with the ability to oxidize lipids might be better able to maintain oxphos than cells without this metabolic flexibility. Finally, our study points to three possible therapeutic targets, namely, the AMPK, mTORC1 and ISR pathways. However, it will be important to understand if the extent of the change in these pathways depends on other aspects of the pathophysiology of FXN-depletion, and if the changes in these pathways are indeed harmful since it is also possible that some changes in signaling benefit the FXN-depleted heart.

METHODS

Mouse model

Mice were used in accordance with mandated standards of care and, use was approved by the Thomas Jefferson University Institutional Animal Care and Use Committee. Mice were housed at 22C, under a 12-hr light-dark cycle (lights on at 07:00). We used a doxycycline-inducible model of FXN knockdown (Chandran et al., 2017). Here, TG mouse (on C56BL/6J background) contain a Tet-On frataxin shRNA expression cassette. Littermates that do not contain the shRNA cassette were used as controls (WT). Doxycycline was administered in the chow (200 p.p.m. in Chow

5SHA, Animal Specialties) to WT and TG mice starting at 9 weeks of age. Only male mice were used for experiments.

Echocardiography

Transthoracic two-dimensional echocardiography was performed using an echocardiographic imaging system (Vevo 2100, VisualSonic, Toronto, Canada) with a 40-MHz probe. Mice were anesthetized through the inhalation of isoflurane (~1–2%); anesthesia was titrated with the goal of equalizing heart rate in all mice. M-mode interrogation was performed in the parasternal short-axis view at the level of the greatest left ventricular end-diastolic dimension. Left ventricular wall thickness and internal dimensions were measured and used for calculation of fraction shortening and ejection fraction values.

Treadmill running

Treadmill running was performed in the early afternoon. Mice were habituated to the Exer3-6 treadmill with shock detector (Columbus Instruments, Columbus, OH) over 2 days. On the first day, mice explored the treadmill, which was not turned on for 15 mins. On the second day, mice ran at 10 m/min for 15 min, with shocks turned on. To test exercise tolerance, mice ran a protocol described in (Frederick, Davis et al., 2015), with a speed increase from 0 to 25 m/min, at 2.5 m/min increments, for a total of 90 minutes, at 0° incline. Exhaustion was defined as 30 consecutive seconds on the shock grid (73 V, 0.97 mA, 1 Hz) with attempting to return to running.

Lactate measurement in blood

A blood sample was obtained from a small nick at the end of the mouse's tail, before running then immediately after the mouse was determined to be exhausted from treadmill running. Lactate content was analyzed using a lactate meter (Nova Biomedical).

Isolation of heart mitochondria

Heart mitochondria were isolated as described in (Ast et al.). All steps were performed on ice or at 4°C. The heart was dissected, washed in heart isolation buffer (HB: 225 mM mannitol, 75 mM sucrose, 20 mM HEPES, 0.1 mM EGTA, pH 7.4), minced with a razor blade, then suspended in HB+0.5% defatted BSA in a glass/Teflon Potter-Elvehjem homogenizer and homogenized (350 rpm, 10 passes). Samples were centrifuged (5 min, 500*g*), the supernatant was centrifuged (10 min, 9000*g*), then the pellet was resuspended in HB devoid of BSA then centrifuged again (10 min, 9000*g*). The final pellet was resuspended in HB (no BSA) in a volume that resulted in a protein concentration of ~20 mg/ml. Protein concentration was determined by bicinchoninic acid (BCA) assay.

Bioenergetics analyses in isolated heart mitochondria

For most experiments, O_2 consumption (JO_2) was measured using the Seahorse XF24 Analyzer (Seahorse Bioscience, Billerica, MA, USA). Isolated mitochondria were studied essentially as we have done previously (Moffat, Bhatia et al., 2014). Each well of the custom microplate contained 10 µg of mitochondria suspend in mitochondria assay medium (MAS; 70 mM sucrose, 22 mM mannitol, 10 mM KH_2PO_4, 5 mM $MgCl_2$, 2 mM Hepes, 1 mM EGTA, 0.2% defatted BSA, pH 7.4 at 37°C). Amount of mitochondria had been optimized such that the O_2 *vs*. time signal was linear under all conditions. The microplate was centrifuged (2000*g*, 20 min, 4°C) to promote adhesion of mitochondria to the plastic. Attachment was verified after centrifugation and again after experiments. Different substrates were tested: malate-pyruvate (5 mM/10 mM), succinate (10 mM + 1 µM rotenone to inhibit Complex I and thereby prevent reverse electron flow through that complex), palmitoyl-L-carnitine – malate (20 µM/1 mM), octanoyl-L-carnitine (200 µM + 1 mM malate). Oligomycin (4 µg/mL) was used to measure non-phosphorylation “leak” respiration JO_2 and the uncoupler FCCP (6.7 µM) was used to measure maximal electron transport chain activity. Antimycin titrations of octanoyl-L-carnitine (200 µM + 1 mM malate) were done in the presence of oligomycin (4 µg/ml) using the Oroboros O2k, with 200 µg of mitochondria per reaction, in MAS.

Fluorometric measurements in isolated mitochondria

Fluorometric measurements of mitochondrial membrane potential ($\Delta\Psi m$) were performed using a multiwavelength-excitation dual-wavelength-emission fluorimeter (DeltaRAM, PTI). Briefly, isolated mitochondria (375 µg) were resuspended in 1.5 ml of intracellular medium containing 120 mM KCl, 10 mM NaCl, 1 mM KH_2PO_4, 20 mM Tris-HEPES at pH 7.2 and

maintained in a stirred thermostated cuvette at 36 °C. TMRM (1μM) was added prior the experiment. Antimycin titrations of octanoyl-L-carnitine (200 μM μM + 1 mM malate) were done in the presence of oligomycin (4 μg/ml). FCCP (6.7 μM) was used to obtain maximal membrane depolarization.

Immunoblot analysis

For western blot analysis, heart was quickly frozen in liquid nitrogen. After that, tissue was homogenized with a lysis buffer containing: NaCl, 150 mM; HEPES 25 mM; EGTA 2.5 mM; Triton 100X 1%; Igepal (10%) 1%; SDS 0.10%; Desoxycholate 0.1%; Glycerol 10%, Protease inhibitor (Roche 11873580001) and Phosphatase inhibitor cocktail (sodium fluoride 200mM, imidazole 200mM, sodium molybedate 115mM, sodium orthovanadate 200mM, sodium tartrate dihydrate 400mM, sodium pyrophosphate 100mM and β-glycerophosphate 100mM), using a glass/Teflon homogenizer at 300 rpm. After that, heart lysates were incubated at 4°C for 45 min, then spin at 12.000 for 20 min. From the supernatant, protein concentration was measured by bicinchoninic acid (BCA) assay. (ThermoFisher Scientific 23228, 1859078). Primary antibodies were used for overnight incubation diluted in TBS-T 1% and are listed in Table 1.

For western blot analysis of mitochondrial proteins, isolated heart mitochondria were lysed in RIPA buffer. Primary antibodies were used for overnight incubation diluted in TBS-T 1% and are listed in Table 2.

Table 1: Primary Antibodies used in heart lysates

Antibody	Catalog Number	Dilution	Host
Phospho-mTOR (Ser2448)	Cell Signaling Technology (CST)-2971	1:1000	Rabbit
mTOR	CST-2972	1:1000	Rabbit
Phospho-RAPTOR (Ser792)	CST-2083	1:1000	Rabbit
RAPTOR	CST-2280	1:1000	Rabbit
Phospho-P70-S6K (Thr389)	CST-9234	1:1000	Rabbit
P70-S6K	CST-9202	1:1000	Rabbit
Phospho-S6 (Ser235/236)	CST-2211	1:1000	Rabbit
S6	CST-2217	1:1000	Rabbit
Phospho-4EBP1 (Thr70)	CST-9455	1:1000	Rabbit
4EBP1	CST-9644	1:1000	Rabbit
Phospho-AMPK (Thr172)	CST-2535	1:1000	Rabbit

AMPKα	CST-2532	1:1000	Rabbit
Phospho-AKT (Thr308) XP	CST-13038	1:1000	Rabbit
Phospho-AKT (Ser473) XP	CST-4060	1:1000	Rabbit
AKT	CST-9272	1:1000	Rabbit
Phospho-eIF2α (Ser51)	CST-3398	1:1000	Rabbit
eIF2α	CST-5324	1:1000	Rabbit
ATF4	Novus Biologicals NB100852	1:500	Goat
BIP	CST-3177	1:1000	Rabbit
Phospho-PERK	CST-3179	1:1000	Rabbit
PERK	CST-5683	1:1000	Rabbit
Catalase	CST-8841	1:1000	Rabbit
Frataxin	Abcam (Ab)175402	1:1000	Rabbit
GRB2	SC-8034	1:1000	Rabbit
GAPDH	Millipore Sigma MAB374	1:5000	Mouse
Transferrin receptor	Thermofisher Scietific H68.4	1:500	Mouse
Ferroportin/FPN1/SLC40A1	Novus Biological NBP1-21502SS	1:1000	Rabbit
FTH	CST-3998	1:1000	Rabbit
Ubiquitin	CST-3936	1:1000	Mouse
K48-linkage specific Polyubiqutin	CST-8081	1:1000	Rabbit
K63-linkage specific Polyubiqutin	CST-5621	1:1000	Rabbit
Anti-Puromycin	Millipore Sigma MABE343	1:5000	Mouse

Table 2: Primary Antibodies used in isolated mitochondria preparations:

Antibody	Catalog Number	Dilution	Host
NDUFA9	Ab14173	1:1000	Mouse
SDHA	Ab14175	1:1000	Mouse
SDHB	Novus Biologicals NBP1-54154SS	1:1000	Rabbit
UQCRC2	Ab14745	1:1000	Mouse
UQCRFS1 (Rieske)	Novus Biologicals NBP1-32367	1:1000	
MTCO2	Ab198286	1:1000	Rabbit
ATP5A	Ab14748	1:1000	Mouse
ETFA	Ab153722	1:1000	Rabbit
ETFDH	Ab131376	1:1000	Mouse
HSP70	ThermoFisher Scientific MA3-008	1:1000	Mouse
Cytochrome c	BD Pharmingen 556433	1:1000	Mouse
Anti 4-Hidroxynonenal (4-HNE)	Ab46545	1:1000	Rabbit
Acetylated Lysine (Ac-Lys)	CST-8081	1:1000	Rabbit

Blue native electrophoresis and in-gel activity

Isolated heart mitochondria (100 µg) were lysed in 4% digitonin in extraction n buffer (30 mM HEPES, 12 % glycerol, 150 mM potassium acetate, 2 mM aminocaproic acid, 2 mM EDTA disodium salt, protease inhibitor tablet (Roche 11873580001), pH 7.4), at 4°C for 30 min with constant shaking at 1500 rpm. The samples were centrifuged at 25000 g, 20 min, 4°C, then 1:400

diluted 5% Coomassie Blue G-250 was added to the supernatant. The samples were then loaded on a gradient gel (NativePAGE™ NovexR 3–12% Bis-Tris). The gel was run overnight in Native PAGE buffers (Invitrogen). The gel for Coomassie blue staining was run in dark blue buffer until the dye front reached 1/3 of the gel (150V) then in light blue buffer for the rest of the time up to 16h (30V). For gels used for in-gel activity, the gel was run first in light blue buffer then in clear buffer (Native PAGE Invitrogen). Following the electrophoresis, the gel was stained with Coomassie Blue R-250 for 30 min, then destained (40% MetOH, 10% acetic acid in water). In-gel activity of complex I, II, and V was run as described (Jha, Wang et al., 2016).

Quantitative polymerase chain reaction

Total RNA was extracted from tissues using Trizol® (Invitrogen, Carlsbad, CA) then treated with RQ1 DNase (Promega, Madison, WI, USA) at 37°C for 30 mins. RNA concentration was measured by Qubit® Fluorometer (Invitrogen, Carlsbad, CA). RNA was reverse transcribed using oligo(dT)20 primers and SuperScript III (Invitrogen, Carlsbad, CA). Primers were designed using Eurofins Primer Design Tool, and checked for specificity and efficiency. Primers sequences are shown below. qPCR reactions were performed using ITaq SYBR green Supermix with ROX (BIO-RAD, Hercules, CA), with 20 ng cDNA/reactions, using an Eppendorf Mastercycler® ep realplex. The ΔΔCt method was used to calculate mRNA levels relative to *Actb* (β-actin). Primers sequences used are listed in table 3.

Table 3: qPCR primers (all are mouse-specific)

Primer name		Sequence
Myh6 (α-MHC)	Forward	CGGAACAAGACAACCTCAAT
	Reverse	TGGCAATGATTTCATCCAGC
Myh7 (β-MHC)	Forward	TTGCTACCCTCAGGTGGCT
	Reverse	CCTTCTCAGACTTCCGCAGG
Cd36	Forward	GGCCAAGCTATTGCGACAT
	Reverse	CAGATCCGAACACAGCGTAGA
Cpt1b	Forward	TGCCTTTACATCGTCTCCAA
	Reverse	AGACCCCGTAGCCATCATC
Acadm (MCAD)	Forward	CATTCCGGAAAGTTGCGGTGG
	Reverse	TAATGGCCGCCACATCAGAG
Slc2a4 (GLUT4)	Forward	TTATTGCAGCGCCTGAGTCT
	Reverse	CAATCACCTTCTGTGGGGCAT
Hk2	Forward	CCGACTCGCCGCAACAAG
	Reverse	ACTCGCCATGTTCTGTCCCAT
Pfkfb1	Forward	TTTCGCCCAGACAACATGGA
	Reverse	TCAAAAACCGCAACGTGACC

Mthfd2	Forward	AGGTCCCAAGCCTTTGAGTT
	Reverse	GTAAGGGAGTGCCGTTGAAA
Psat1	Forward	AGTGGAGCGCCAGAATAGAA
	Reverse	CTTCGGTTGTGACAGCGTTA
Phgdh	Forward	GACCCCATCATCTCTCCTGA
	Reverse	GCACACCTTTCTTGCACTGA
Atf2	Forward	TGTCATTGTGGCTGATCAGACTC
	Reverse	GTGTTGCAAGAGGGGACAAATC
Atf3	Forward	CCAGAATAAACACCTCTGCCATCG
	Reverse	CTTCAGCTCAGCATTCACACTCTC
Atf4	Forward	CCACCATGGCGTATTAGAGG
	Reverse	GTCCGTTACAGCAACACTGC
Atf5	Forward	CTGGGAACCCCTGTGGATTAAA
	Reverse	GCAGCGTGGAAGATTGTTCA
Slc7a5	Forward	TGCAGCCATGACCCTAACAG
	Reverse	AACAATGGGGACAGACCAGG
Asns	Forward	TGGCTGCCTTTTATCAGGGG
	Reverse	CAGATGCCCGAACTGTCGTA
Fgf21	Forward	ATGGAATGGATGAGATCTAGAGTTGG
	Reverse	TCTTGGTGGTCATCTGTGTAGAGG
Gdf15	Forward	GAGCTACGGGGTCGCTTC
	Reverse	GGGACCCCAATCTCACCT
Clpp	Forward	CCAAGCACACCAAACAGAG
	Reverse	GGACCAGAACCTTGTCTAAGAT
Lonp1	Forward	CTGTGTTCCCGCGCTTTATC
	Reverse	GCCAGTGACAATCATTCGCAA
Fbxo32 (Atrogin1)	Forward	ACCTGCTGGTGGAAAACATC
	Reverse	CTTCGTGTTCCTTGCACATC
Trim63 (MuRF1)	Forward	AAGGAGCGCCATGGGATACTG
	Reverse	GTCACGCACGATTTCCC
Tfrc	Forward	AGCCAGATCAGCATTCTCTAACT
	Reverse	GCCTTCATGTTATTGTCGGCAT
Actb (β-actin)	Forward	CAACACCCCAGCCATG
	Reverse	GTCACGCACGATTTCCC

Global protein synthesis

To measure the rate of global protein synthesis, we used an in vivo SUnSET assay (Schmidt et al., 2009). For this study, a sterilized puromycin (Sigma, 8833) solution in PBS (4mg/mL), was injected intraperitoneally. The volume of the puromycin injection was calculated based on the body weight of the mouse, for a final concentration of 0.04 μmol/g. Thirty minutes after the injection, animals were sacrificed to collect tissue samples for biochemical detection of incorporated puromycin by western blot.

Histology

Hematoxylin/eosin (H&E), Masson's Trichrome and Perls' Prussian Blue staining were performed at the translational research /pathology shared resource at Thomas Jefferson University. Bright field images were acquired using an Olympus CKX41 inverted microscope and cellSens Standard software. Images were analyzed using Image J.

Quantification and statistical analysis

Data analysis was performed using GraphPad Prism 8.2.1 Software. Unpaired Student's *t* test for comparison of two means, or one-way analysis of variance followed by Tukey post-hoc comparisons, for multiple comparisons, were performed as appropriate. P value < 0.05 was considered significant. In all cases, data not indicated as significant should be considered not statistically different. Details specific for a given measurement, including sample sizes, are provided in Results and the figure legends

Data and code availability

Data and Code Availability Statement: The published article includes all [datasets/code] generated or analyzed during this study.

ACKNOWLEDGEMENTS

The authors thank Drs. Vijay Chandran (University of Florida) and Daniel Geschwind (UCLA) for providing the mouse model. Studies were funded by grants from the Friedreich's Ataxia Research Alliance (to ELS) and NIH R01 GM123771 (to ELS).

AUTHOR CONTRIBUTIONS

Conceptualization: C. V-T., E.L.S.; Investigation: C. V-T., M.P., A.S., C.B., L.A.-P., N.W.; Writing: C. V-T., E.L.S.; Funding Acquisition: E.L.S..

DECLARATION OF INTERESTS

The authors declare no competing interests.

REFERENCES

Anderson CP, Shen M, Eisenstein RS, Leibold EA (2012) Mammalian iron metabolism and its control by iron regulatory proteins. *Biochim Biophys Acta* 1823: 1468-83

Ast T, Meisel JD, Patra S, Wang H, Grange RMH, Kim SH, Calvo SE, Orefice LL, Nagashima F, Ichinose F, Zapol WM, Ruvkun G, Barondeau DP, Mootha VK (2019) Hypoxia Rescues Frataxin Loss by Restoring Iron Sulfur Cluster Biogenesis. *Cell* 177: 1507-1521 e16

Bao XR, Ong SE, Goldberger O, Peng J, Sharma R, Thompson DA, Vafai SB, Cox AG, Marutani E, Ichinose F, Goessling W, Regev A, Carr SA, Clish CB, Mootha VK (2016) Mitochondrial dysfunction remodels one-carbon metabolism in human cells. *Elife* 5

Belbellaa B, Reutenauer L, Monassier L, Puccio H (2019) Correction of half the cardiomyocytes fully rescue Friedreich ataxia mitochondrial cardiomyopathy through cell-autonomous mechanisms. *Hum Mol Genet* 28: 1274-1285

Boukens BJ, Rivaud MR, Rentschler S, Coronel R (2014) Misinterpretation of the mouse ECG: 'musing the waves of Mus musculus'. *J Physiol* 592: 4613-26

Chandran V, Gao K, Swarup V, Versano R, Dong H, Jordan MC, Geschwind DH (2017) Inducible and reversible phenotypes in a novel mouse model of Friedreich's Ataxia. *Elife* 6

Civiletto G, Dogan SA, Cerutti R, Fagiolari G, Moggio M, Lamperti C, Beninca C, Viscomi C, Zeviani M (2018) Rapamycin rescues mitochondrial myopathy via coordinated activation of autophagy and lysosomal biogenesis. *EMBO Mol Med* 10

Costa-Mattioli M, Walter P (2020) The integrated stress response: From mechanism to disease. *Science* 368

Crooks DR, Maio N, Lane AN, Jarnik M, Higashi RM, Haller RG, Yang Y, Fan TW, Linehan WM, Rouault TA (2018) Acute loss of iron-sulfur clusters results in metabolic reprogramming and generation of lipid droplets in mammalian cells. *J Biol Chem* 293: 8297-8311

Dogan SA, Cerutti R, Beninca C, Brea-Calvo G, Jacobs HT, Zeviani M, Szibor M, Viscomi C (2018) Perturbed Redox Signaling Exacerbates a Mitochondrial Myopathy. *Cell Metab* 28: 764-775 e5

Ellis JM, Mentock SM, Depetrillo MA, Koves TR, Sen S, Watkins SM, Muoio DM, Cline GW, Taegtmeyer H, Shulman GI, Willis MS, Coleman RA (2011) Mouse cardiac acyl coenzyme a synthetase 1 deficiency impairs Fatty Acid oxidation and induces cardiac hypertrophy. *Mol Cell Biol* 31: 1252-62

Fornasiero EF, Mandad S, Wildhagen H, Alevra M, Rammner B, Keihani S, Opazo F, Urban I, Ischebeck T, Sakib MS, Fard MK, Kirli K, Centeno TP, Vidal RO, Rahman RU, Benito E, Fischer A, Dennerlein S, Rehling P, Feussner I et al. (2018) Precisely measured protein lifetimes in the mouse brain reveal differences across tissues and subcellular fractions. *Nat Commun* 9: 4230

Forsstrom S, Jackson CB, Carroll CJ, Kuronen M, Pirinen E, Pradhan S, Marmyleva A, Auranen M, Kleine IM, Khan NA, Roivainen A, Marjamaki P, Liljenback H, Wang L, Battersby BJ, Richter U, Velagapudi V, Nikkanen J, Euro L, Suomalainen A (2019) Fibroblast Growth Factor 21 Drives Dynamics of Local and Systemic Stress Responses in Mitochondrial Myopathy with mtDNA Deletions. *Cell Metab* 30: 1040-1054 e7

Frederick DW, Davis JG, Davila A, Jr., Agarwal B, Michan S, Puchowicz MA, Nakamaru-Ogiso E, Baur JA (2015) Increasing NAD synthesis in muscle via nicotinamide phosphoribosyltransferase is not sufficient to promote oxidative metabolism. *J Biol Chem* 290: 1546-58

Guo X, Aviles G, Liu Y, Tian R, Unger BA, Lin YT, Wiita AP, Xu K, Correia MA, Kampmann M (2020) Mitochondrial stress is relayed to the cytosol by an OMA1-DELE1-HRI pathway. *Nature* 579: 427-432

Han AP, Yu C, Lu L, Fujiwara Y, Browne C, Chin G, Fleming M, Leboulch P, Orkin SH, Chen JJ (2001) Heme-regulated eIF2alpha kinase (HRI) is required for translational regulation and survival of erythroid precursors in iron deficiency. *EMBO J* 20: 6909-18

Hawley SA, Ross FA, Gowans GJ, Tibarewal P, Leslie NR, Hardie DG (2014) Phosphorylation by AKT within the ST loop of AMPK-alpha1 down-regulates its activation in tumour cells. *Biochem J* 459: 275-87

Herron TJ, Korte FS, McDonald KS (2001) Loaded shortening and power output in cardiac myocytes are dependent on myosin heavy chain isoform expression. *Am J Physiol Heart Circ Physiol* 281: H1217-22
Herron TJ, McDonald KS (2002) Small amounts of alpha-myosin heavy chain isoform expression significantly increase power output of rat cardiac myocyte fragments. *Circ Res* 90: 1150-2
Huang ML, Sivagurunathan S, Ting S, Jansson PJ, Austin CJ, Kelly M, Semsarian C, Zhang D, Richardson DR (2013) Molecular and functional alterations in a mouse cardiac model of Friedreich ataxia: activation of the integrated stress response, eIF2alpha phosphorylation, and the induction of downstream targets. *Am J Pathol* 183: 745-57
Jha P, Wang X, Auwerx J (2016) Analysis of Mitochondrial Respiratory Chain Supercomplexes Using Blue Native Polyacrylamide Gel Electrophoresis (BN-PAGE). *Curr Protoc Mouse Biol* 6: 1-14
Johnson SC, Yanos ME, Bitto A, Castanza A, Gagnidze A, Gonzalez B, Gupta K, Hui J, Jarvie C, Johnson BM, Letexier N, McCanta L, Sangesland M, Tamis O, Uhde L, Van Den Ende A, Rabinovitch PS, Suh Y, Kaeberlein M (2015) Dose-dependent effects of mTOR inhibition on weight and mitochondrial disease in mice. *Front Genet* 6: 247
Johnson SC, Yanos ME, Kayser EB, Quintana A, Sangesland M, Castanza A, Uhde L, Hui J, Wall VZ, Gagnidze A, Oh K, Wasko BM, Ramos FJ, Palmiter RD, Rabinovitch PS, Morgan PG, Sedensky MM, Kaeberlein M (2013) mTOR inhibition alleviates mitochondrial disease in a mouse model of Leigh syndrome. *Science* 342: 1524-8
Karamanlidis G, Lee CF, Garcia-Menendez L, Kolwicz SC, Jr., Suthammarak W, Gong G, Sedensky MM, Morgan PG, Wang W, Tian R (2013) Mitochondrial complex I deficiency increases protein acetylation and accelerates heart failure. *Cell Metab* 18: 239-50
Khan NA, Nikkanen J, Yatsuga S, Jackson C, Wang L, Pradhan S, Kivela R, Pessia A, Velagapudi V, Suomalainen A (2017) mTORC1 Regulates Mitochondrial Integrated Stress Response and Mitochondrial Myopathy Progression. *Cell Metab* 26: 419-428 e5
Kipps A, Alexander M, Colan SD, Gauvreau K, Smoot L, Crawford L, Darras BT, Blume ED (2009) The longitudinal course of cardiomyopathy in Friedreich's ataxia during childhood. *Pediatr Cardiol* 30: 306-10
Kovacic S, Soltys CL, Barr AJ, Shiojima I, Walsh K, Dyck JR (2003) AKT activity negatively regulates phosphorylation of AMP-activated protein kinase in the heart. *J Biol Chem* 278: 39422-7
Kuhl I, Miranda M, Atanassov I, Kuznetsova I, Hinze Y, Mourier A, Filipovska A, Larsson NG (2017) Transcriptomic and proteomic landscape of mitochondrial dysfunction reveals secondary coenzyme Q deficiency in mammals. *Elife* 6
Lim SC, Friemel M, Marum JE, Tucker EJ, Bruno DL, Riley LG, Christodoulou J, Kirk EP, Boneh A, DeGennaro CM, Springer M, Mootha VK, Rouault TA, Leimkuhler S, Thorburn DR, Compton AG (2013) Mutations in LYRM4, encoding iron-sulfur cluster biogenesis factor ISD11, cause deficiency of multiple respiratory chain complexes. *Hum Mol Genet* 22: 4460-73
Liu GY, Sabatini DM (2020) mTOR at the nexus of nutrition, growth, ageing and disease. *Nat Rev Mol Cell Biol* 21: 183-203
Martin AS, Abraham DM, Hershberger KA, Bhatt DP, Mao L, Cui H, Liu J, Liu X, Muehlbauer MJ, Grimsrud PA, Locasale JW, Payne RM, Hirschey MD (2017) Nicotinamide mononucleotide requires SIRT3 to improve cardiac function and bioenergetics in a Friedreich's ataxia cardiomyopathy model. *JCI Insight* 2
Mik EG, Ince C, Eerbeek O, Heinen A, Stap J, Hooibrink B, Schumacher CA, Balestra GM, Johannes T, Beek JF, Nieuwenhuis AF, van Horssen P, Spaan JA, Zuurbier CJ (2009) Mitochondrial oxygen tension within the heart. *J Mol Cell Cardiol* 46: 943-51
Moffat C, Bhatia L, Nguyen T, Lynch P, Wang M, Wang D, Ilkayeva OR, Han X, Hirschey MD, Claypool SM, Seifert EL (2014) Acyl-CoA thioesterase-2 facilitates mitochondrial fatty acid oxidation in the liver. *J Lipid Res* 55: 2458-70
Navarro-Sastre A, Tort F, Stehling O, Uzarska MA, Arranz JA, Del Toro M, Labayru MT, Landa J, Font A, Garcia-Villoria J, Merinero B, Ugarte M, Gutierrez-Solana LG, Campistol J, Garcia-Cazorla A, Vaquerizo J,

Riudor E, Briones P, Elpeleg O, Ribes A et al. (2011) A fatal mitochondrial disease is associated with defective NFU1 function in the maturation of a subset of mitochondrial Fe-S proteins. *Am J Hum Genet* 89: 656-67

Nikkanen J, Forsstrom S, Euro L, Paetau I, Kohnz RA, Wang L, Chilov D, Viinamaki J, Roivainen A, Marjamaki P, Liljenback H, Ahola S, Buzkova J, Terzioglu M, Khan NA, Pirnes-Karhu S, Paetau A, Lonnqvist T, Sajantila A, Isohanni P et al. (2016) Mitochondrial DNA Replication Defects Disturb Cellular dNTP Pools and Remodel One-Carbon Metabolism. *Cell Metab* 23: 635-48

Pakos-Zebrucka K, Koryga I, Mnich K, Ljujic M, Samali A, Gorman AM (2016) The integrated stress response. *EMBO Rep* 17: 1374-1395

Perdomini M, Belbellaa B, Monassier L, Reutenauer L, Messaddeq N, Cartier N, Crystal RG, Aubourg P, Puccio H (2014) Prevention and reversal of severe mitochondrial cardiomyopathy by gene therapy in a mouse model of Friedreich's ataxia. *Nat Med* 20: 542-7

Pereira RO, Tadinada SM, Zasadny FM, Oliveira KJ, Pires KMP, Olvera A, Jeffers J, Souvenir R, McGlauflin R, Seei A, Funari T, Sesaki H, Potthoff MJ, Adams CM, Anderson EJ, Abel ED (2017) OPA1 deficiency promotes secretion of FGF21 from muscle that prevents obesity and insulin resistance. *EMBO J* 36: 2126-2145

Quiros PM, Prado MA, Zamboni N, D'Amico D, Williams RW, Finley D, Gygi SP, Auwerx J (2017) Multi-omics analysis identifies ATF4 as a key regulator of the mitochondrial stress response in mammals. *J Cell Biol* 216: 2027-2045

Reetz K, Dogan I, Costa AS, Dafotakis M, Fedosov K, Giunti P, Parkinson MH, Sweeney MG, Mariotti C, Panzeri M, Nanetti L, Arpa J, Sanz-Gallego I, Durr A, Charles P, Boesch S, Nachbauer W, Klopstock T, Karin I, Depondt C et al. (2015) Biological and clinical characteristics of the European Friedreich's Ataxia Consortium for Translational Studies (EFACTS) cohort: a cross-sectional analysis of baseline data. *Lancet Neurol* 14: 174-82

Rotig A, de Lonlay P, Chretien D, Foury F, Koenig M, Sidi D, Munnich A, Rustin P (1997) Aconitase and mitochondrial iron-sulphur protein deficiency in Friedreich ataxia. *Nat Genet* 17: 215-7

Schmidt EK, Clavarino G, Ceppi M, Pierre P (2009) SUnSET, a nonradioactive method to monitor protein synthesis. *Nat Methods* 6: 275-7

Schoenfeld RA, Napoli E, Wong A, Zhan S, Reutenauer L, Morin D, Buckpitt AR, Taroni F, Lonnerdal B, Ristow M, Puccio H, Cortopassi GA (2005) Frataxin deficiency alters heme pathway transcripts and decreases mitochondrial heme metabolites in mammalian cells. *Hum Mol Genet* 14: 3787-99

Seznec H, Simon D, Monassier L, Criqui-Filipe P, Gansmuller A, Rustin P, Koenig M, Puccio H (2004) Idebenone delays the onset of cardiac functional alteration without correction of Fe-S enzymes deficit in a mouse model for Friedreich ataxia. *Hum Mol Genet* 13: 1017-24

Siegmund SE, Yang H, Sharma R, Javors M, Skinner O, Mootha V, Hirano M, Schon EA (2017) Low-dose rapamycin extends lifespan in a mouse model of mtDNA depletion syndrome. *Hum Mol Genet* 26: 4588-4605

Soltys CL, Kovacic S, Dyck JR (2006) Activation of cardiac AMP-activated protein kinase by LKB1 expression or chemical hypoxia is blunted by increased AKT activity. *Am J Physiol Heart Circ Physiol* 290: H2472-9

St John Sutton M, Ky B, Regner SR, Schadt K, Plappert T, He J, D'Souza B, Lynch DR (2014) Longitudinal strain in Friedreich Ataxia: a potential marker for early left ventricular dysfunction. *Echocardiography* 31: 50-7

Stram AR, Wagner GR, Fogler BD, Pride PM, Hirschey MD, Payne RM (2017) Progressive mitochondrial protein lysine acetylation and heart failure in a model of Friedreich's ataxia cardiomyopathy. *PLoS One* 12: e0178354

Suomalainen A, Elo JM, Pietilainen KH, Hakonen AH, Sevastianova K, Korpela M, Isohanni P, Marjavaara SK, Tyni T, Kiuru-Enari S, Pihko H, Darin N, Ounap K, Kluijtmans LA, Paetau A, Buzkova J, Bindoff LA,

Annunen-Rasila J, Uusimaa J, Rissanen A et al. (2011) FGF-21 as a biomarker for muscle-manifesting mitochondrial respiratory chain deficiencies: a diagnostic study. *Lancet Neurol* 10: 806-18

Szczepanowska K, Senft K, Heidler J, Herholz M, Kukat A, Hohne MN, Hofsetz E, Becker C, Kaspar S, Giese H, Zwicker K, Guerrero-Castillo S, Baumann L, Kauppila J, Rumyantseva A, Muller S, Frese CK, Brandt U, Riemer J, Wittig I et al. (2020) A salvage pathway maintains highly functional respiratory complex I. *Nat Commun* 11: 1643

Tsou AY, Paulsen EK, Lagedrost SJ, Perlman SL, Mathews KD, Wilmot GR, Ravina B, Koeppen AH, Lynch DR (2011) Mortality in Friedreich ataxia. *J Neurol Sci* 307: 46-9

Tyynismaa H, Carroll CJ, Raimundo N, Ahola-Erkkila S, Wenz T, Ruhanen H, Guse K, Hemminki A, Peltola-Mjosund KE, Tulkki V, Oresic M, Moraes CT, Pietilainen K, Hovatta I, Suomalainen A (2010) Mitochondrial myopathy induces a starvation-like response. *Hum Mol Genet* 19: 3948-58

Varghese J, James J, Vaulont S, McKie A, Jacob M (2018) Increased intracellular iron in mouse primary hepatocytes in vitro causes activation of the AKT pathway but decreases its response to insulin. *Biochim Biophys Acta Gen Subj* 1862: 1870-1882

Viscomi C, Bottani E, Civiletto G, Cerutti R, Moggio M, Fagiolari G, Schon EA, Lamperti C, Zeviani M (2011) In vivo correction of COX deficiency by activation of the AMPK/PGC-1alpha axis. *Cell Metab* 14: 80-90

Wagner GR, Pride PM, Babbey CM, Payne RM (2012) Friedreich's ataxia reveals a mechanism for coordinate regulation of oxidative metabolism via feedback inhibition of the SIRT3 deacetylase. *Hum Mol Genet* 21: 2688-97

Wende AR, Brahma MK, McGinnis GR, Young ME (2017) Metabolic Origins of Heart Failure. *JACC Basic Transl Sci* 2: 297-310

Wojtczak L, Schonfeld P (1993) Effect of fatty acids on energy coupling processes in mitochondria. *Biochim Biophys Acta* 1183: 41-57

Zheng X, Boyer L, Jin M, Kim Y, Fan W, Bardy C, Berggren T, Evans RM, Gage FH, Hunter T (2016) Alleviation of neuronal energy deficiency by mTOR inhibition as a treatment for mitochondria-related neurodegeneration. *Elife* 5

Figure 1

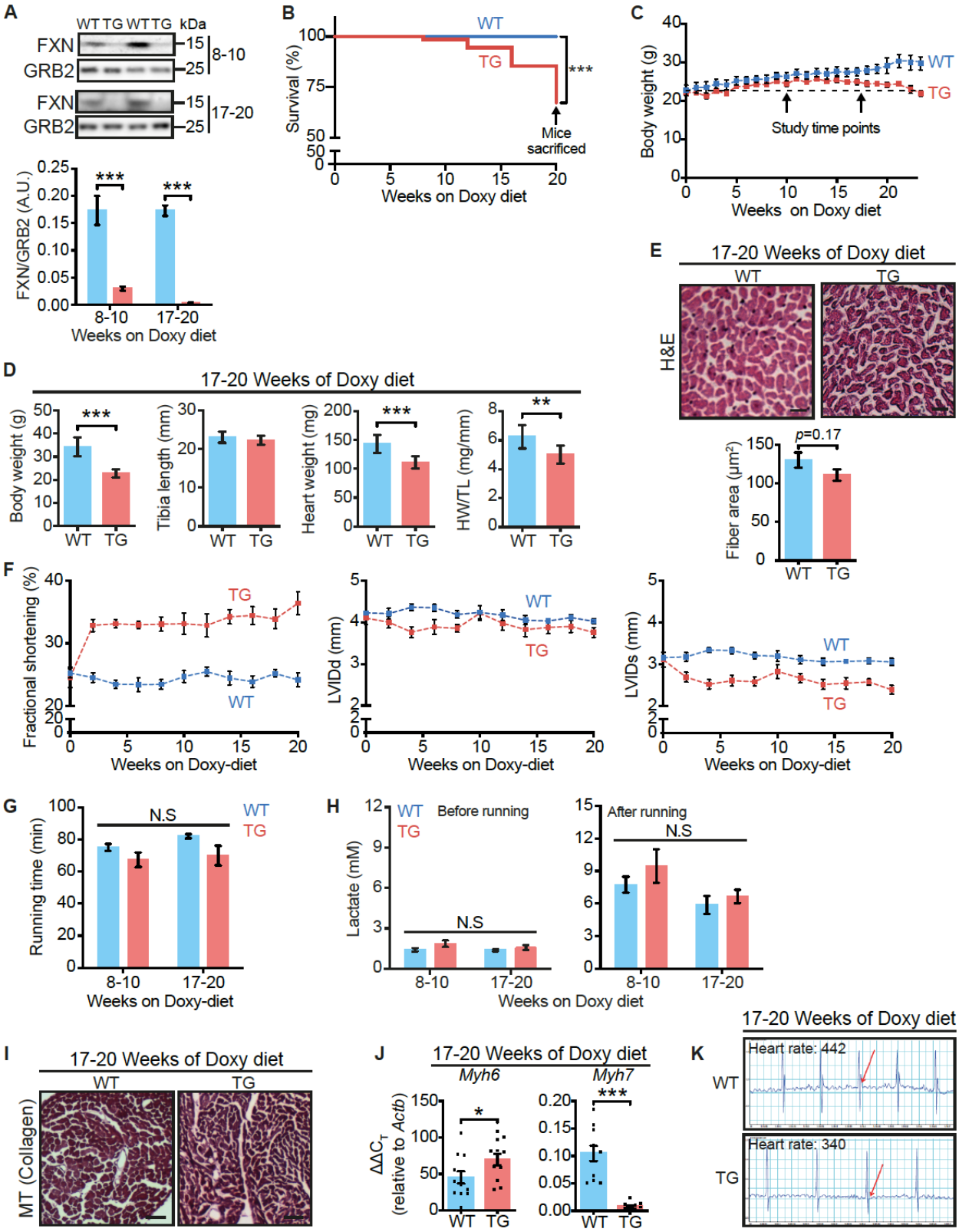
A
WT TG WT TG kDa
FXN
GRB2
FXN
GRB2
15
25
15
25
8-10
17-20
FXN/GRB2 (A.U.)
***
***
8-10
17-20
Weeks on Doxy diet
B
WT
TG
Survival (%)
***
Mice sacrificed
Weeks on Doxy diet
C
Body weight (g)
WT
TG
Study time points
Weeks on Doxy diet
D
17-20 Weeks of Doxy diet
Body weight (g)
Tibia length (mm)
Heart weight (mg)
HW/TL (mg/mm)
WT TG
E
17-20 Weeks of Doxy diet
WT
TG
H&E
Fiber area (μm²)
p=0.17
F
Fractional shortening (%)
LVIDd (mm)
LVIDs (mm)
Weeks on Doxy-diet
G
N.S
WT
TG
Running time (min)
8-10
17-20
Weeks on Doxy-diet
H
WT
TG
Before running
After running
N.S
Lactate (mM)
Weeks on Doxy diet
I
17-20 Weeks of Doxy diet
WT
TG
MT (Collagen)
J
17-20 Weeks of Doxy diet
Myh6
Myh7
ΔΔC_T (relative to Actb)
*
***
WT TG
K
17-20 Weeks of Doxy diet
Heart rate: 442
Heart rate: 340
WT
TG

Figure 1: FXN-depleted hearts exhibit compensated contractility and aerobic capacity, but abnormal morphology and rate. (A) Representative immunoblots of FXN and GRB2 (loading control) levels in heart mitochondria from WT and TG mice from 8-10 and 17-20 weeks of Doxy diet. **(B)** Survival rate (n=29 WT and 20 TG mice, ***p<0.001: Curve comparison, Gehan-Breslow-Wilcoxon test), and **(C)** body weight of WT and TG mice over the course of during Doxy feeding. **(D)** Body weight, tibia length (TL), heart weight (HW), and tibia length to heart weight ratio (HW/TL) of WT and TG mice after 17-20 weeks of Doxy feeding (n=7/genotype, **p<0.01, ***p<0.001) **(E)** *Upper:* Example of histology showing cross-sections of heart (WT and TG from 17-20 weeks of Doxy) stained with H&E to evaluate cross sectional area of cardiac fibers (*lower*) (n= 7 WT and 4 TG). **(F)** Serial echocardiographic evaluation of WT and TG mice during Doxy-feeding. Fractional shortening (FS), left ventricular inner diameter at end-diastole (LVIDd) and at end-systole (LVIDs), were measured (0-18 weeks of Doxy: n=5/genotype; 20 weeks of Doxy: n=4/genotype). **(G)** Treadmill running time during an endurance protocol. (8-10 weeks: n=6/genotype; 17-20 weeks: n=4/genotype). **(H)** Blood lactate levels, before and after running the treadmill running (8-10 weeks: n=6/genotype; 17-20 weeks: n=4/genotype). **(I)** Cross-sections from heart (WT and TG from 17-20 weeks of Doxy) stained with Masson's trichrome to evaluate fibrosis (n= 7 WT/4 TG). **(J)** Transcripts values ($\Delta\Delta C_T$) of *Myh6* (α-MHC) and *Myh7* (β-MHC) (n=11-12 per genotype, *p<0.05, ***p<0.001), normalized to *Actb* (β-actin). **(K)** Representative ECG traces from WT and TG mice after 17-20 weeks of Doxy feeding. Red arrows indicate absence of J-wave. In all cases, values represent the mean ± s.e.m. Statistical analysis is by unpaired t-test, except where otherwise indicated.

Figure 2

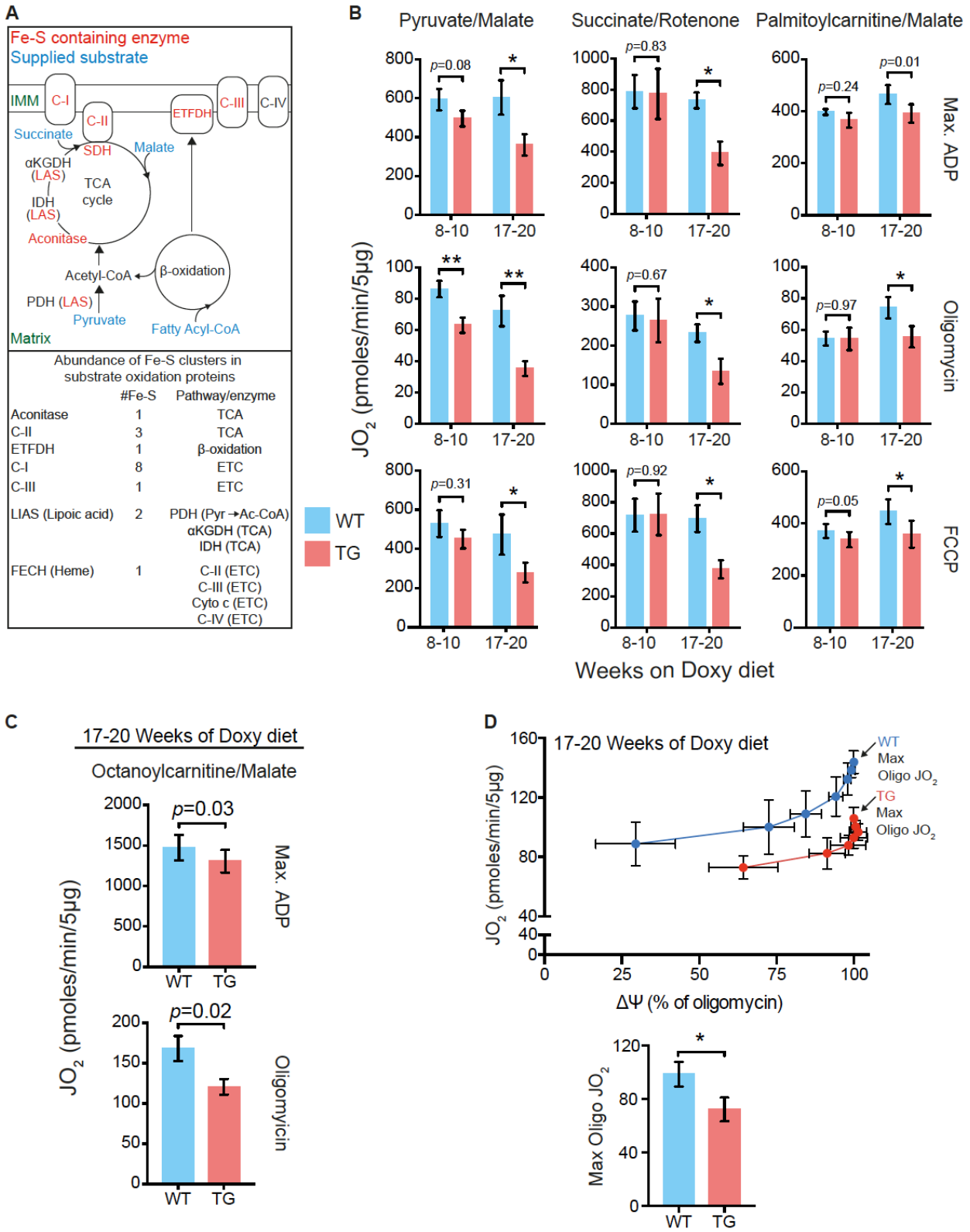
A
Fe-S containing enzyme
Supplied substrate
IMM
C-I
C-II
ETFDH
C-III
C-IV
Succinate
SDH
Malate
αKGDH (LAS)
TCA cycle
IDH (LAS)
Aconitase
Acetyl-CoA
β-oxidation
PDH (LAS)
Pyruvate
Fatty Acyl-CoA
Matrix
Abundance of Fe-S clusters in substrate oxidation proteins
#Fe-S
Pathway/enzyme
Aconitase 1 TCA
C-II 3 TCA
ETFDH 1 β-oxidation
C-I 8 ETC
C-III 1 ETC
LIAS (Lipoic acid) 2 PDH (Pyr→Ac-CoA) αKGDH (TCA) IDH (TCA)
FECH (Heme) 1 C-II (ETC) C-III (ETC) Cyto c (ETC) C-IV (ETC)
B
Pyruvate/Malate
Succinate/Rotenone
Palmitoylcarnitine/Malate
Max. ADP
Oligomycin
FCCP
JO2 (pmoles/min/5µg)
8-10
17-20
Weeks on Doxy diet
WT
TG
C
17-20 Weeks of Doxy diet
Octanoylcarnitine/Malate
Max. ADP
Oligomycin
D
17-20 Weeks of Doxy diet
WT Max Oligo JO2
TG Max Oligo JO2
ΔΨ (% of oligomycin)
Max Oligo JO2

Figure 2: Selective suppression of substrate oxidation in TG heart mitochondria. (A) *Upper*: Schematic diagram showing Fe-S cluster containing enzymes and substrates supplied in bioenergetics experiments. *Lower*: List of Fe-S cluster containing complexes/enzymes with corresponding number of Fe-S clusters and associated metabolic pathway or enzyme. ETFDH: Electron transfer flavoprotein dehydrogenase, LIAS: Lipoic acid synthetase, FECH: Ferrochelatase, PDH: Pyruvate dehydrogenase, αKGDH: α-ketoglutarate dehydrogenase, IDH: Isocitrate dehydrogenase, Cyto c: Cytochrome c. C-I, C-II, CIII and C-IV are mitochondrial respiratory complexes I, II, III and IV, respectively. Pyr: Pyruvate, Ac-CoA: Acetyl-CoA. **(B)** Oxygen consumption rate (JO_2) measurements from isolated heart mitochondria from WT and TG mice (8-10 and 17-20 of Doxy diet), using pyruvate (10 mM) and malate (5 mM), succinate (10 mM + 1 μM rotenone) and palmitoyl-L-carnitine (20 μM) and malate (1 mM), as substrates. (8-10 weeks Doxy: n=6/genotype; 17-20 weeks Doxy: n=6/genotype; *p<0.05, **p<0.01). **(C)** JO_2 using octanoyl-L-carnitine (200 μM) with 1mM malate, between WT and TG heart mitochondria) (n=4/genotype). **(D)** Antimycin titration of octanoyl-L-carnitine, in the presence of oligomycin, to evaluate proton leak JO_2 as a function of membrane potential (ΔΨm). *Lower panel*: Maximal Oligomycin JO_2 values for WT and TG calculated from values indicated by the arrows on the JO_2 vs. ΔΨm plot: these JO_2 values correspond to similar values of ΔΨm (n=3/genotype, *p<0.05). In all experiments, values represent the mean ± s.e.m. Statistical analysis is by unpaired t-test. Analysis of time effect on JO_2 measurements is provided in Figure S2.

Figure 3

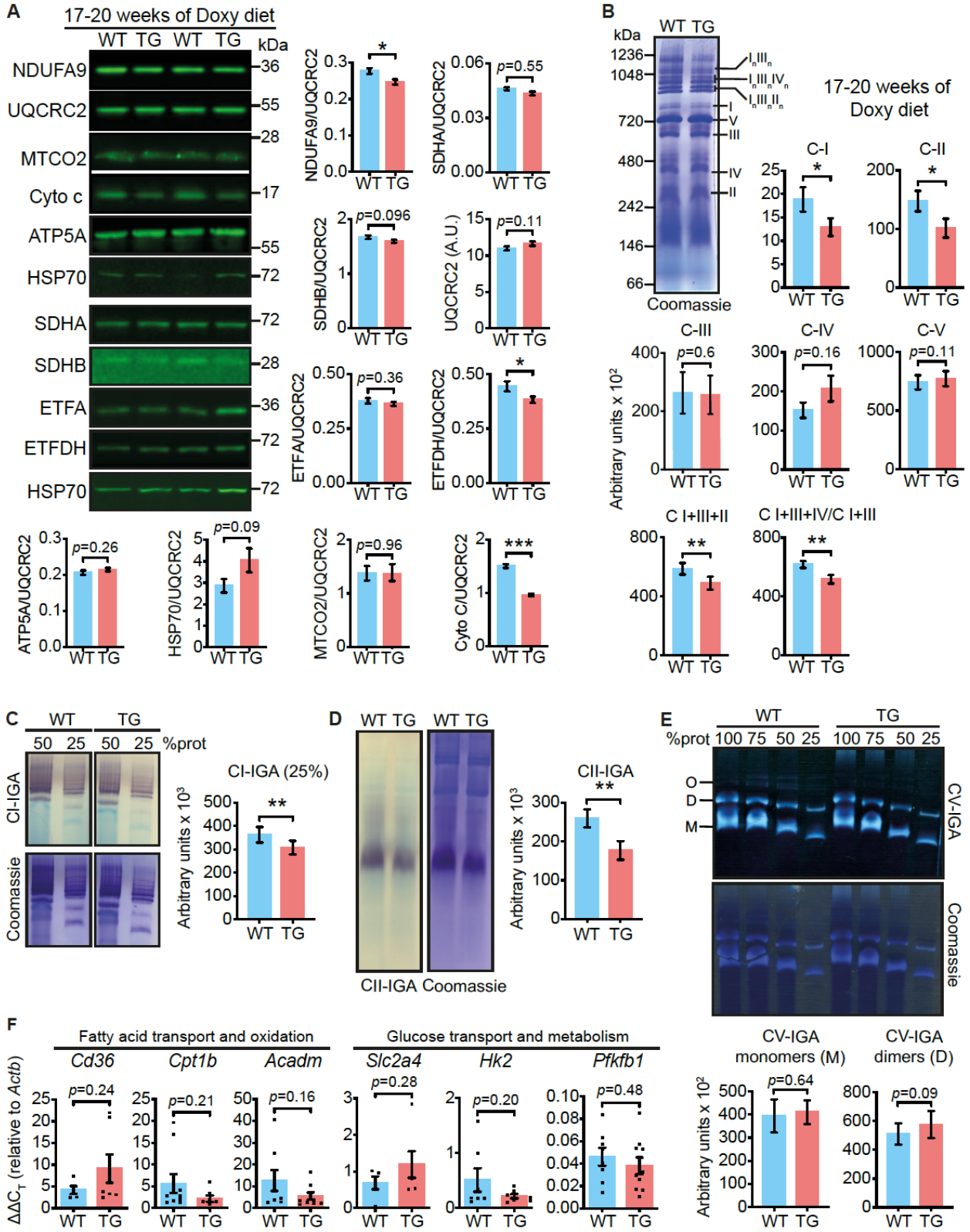
A
17-20 weeks of Doxy diet
WT TG WT TG
kDa
NDUFA9
UQCRC2
MTCO2
Cyto c
ATP5A
HSP70
SDHA
SDHB
ETFA
ETFDH
HSP70
36
55
28
17
55
72
72
28
36
72
72
NDUFA9/UQCRC2
SDHA/UQCRC2
SDHB/UQCRC2
UQCRC2 (A.U.)
ETFA/UQCRC2
ETFDH/UQCRC2
ATP5A/UQCRC2
HSP70/UQCRC2
MTCO2/UQCRC2
Cyto C/UQCRC2
p=0.55
p=0.096
p=0.11
p=0.36
p=0.26
p=0.09
p=0.96
B
WT TG
kDa
1236
1048
720
480
242
146
66
Coomassie
17-20 weeks of Doxy diet
C-I
C-II
C-III
C-IV
C-V
C I+III+II
C I+III+IV/C I+III
Arbitrary units x 10²
p=0.6
p=0.16
p=0.11
C
WT TG
50 25 50 25 %prot
CI-IGA
Coomassie
CI-IGA (25%)
Arbitrary units x 10³
D
WT TG WT TG
CII-IGA Coomassie
CII-IGA
E
WT TG
%prot 100 75 50 25 100 75 50 25
O
D
M
CV-IGA
Coomassie
F
Fatty acid transport and oxidation
Glucose transport and metabolism
Cd36
Cpt1b
Acadm
Slc2a4
Hk2
Pfkfb1
ΔΔC_T (relative to Actb)
p=0.24
p=0.21
p=0.16
p=0.28
p=0.20
p=0.48
CV-IGA monomers (M)
CV-IGA dimers (D)
p=0.64
p=0.09
WT TG

Figure 3: FXN-depleted mitochondria exhibit defects in ETC complex and supercomplex abundance and activity. (A) Representative immunoblots of electron transport chain subunits from isolated heart mitochondria from WT and TG mice (17-20 weeks of Doxy diet) (n=11-16/genotype, *p<0.05, **p<0.01, *p<0.001). Protein levels are displayed in bar graphs, normalized to UQCRC2. **(B)** Representative BN-PAGE gel from isolated heart mitochondria of WT and TG mice (17-20 weeks of Doxy feeding). Complex (C) and supercomplex (SC) levels are displayed in the bar graphs (n=5WT/TG, *p<0.05, **p<0.01). **(C)** Complex I (CI) in-gel activity (IGA) and Coomassie staining; CI-IGA (25% protein loaded per lane) is displayed in the bar graph (*right*) (n=5/genotype, *p<0.05, **p<0.01). **(D)** Complex II (CII)-IGA and Coomassie staining; CII-IGA (25 min reaction) is displayed in the bar graph (*right*) (n=5/genotype, *p<0.05, **p<0.01). **(E)** Complex V (CV)-IGA and Coomassie staining; CV-IGA of monomers (M) and dimers (D) is displayed in the bar graphs (*lower*) (n=3/genotype). **(F)** $\Delta\Delta C_T$ values of transcripts involved in fatty acid and glucose oxidation and transport, normalized to *Actb* (β-actin) (n=8/genotype). All values represent the mean ± s.e.m. Statistical analysis was by unpaired t-test.

Figure 4

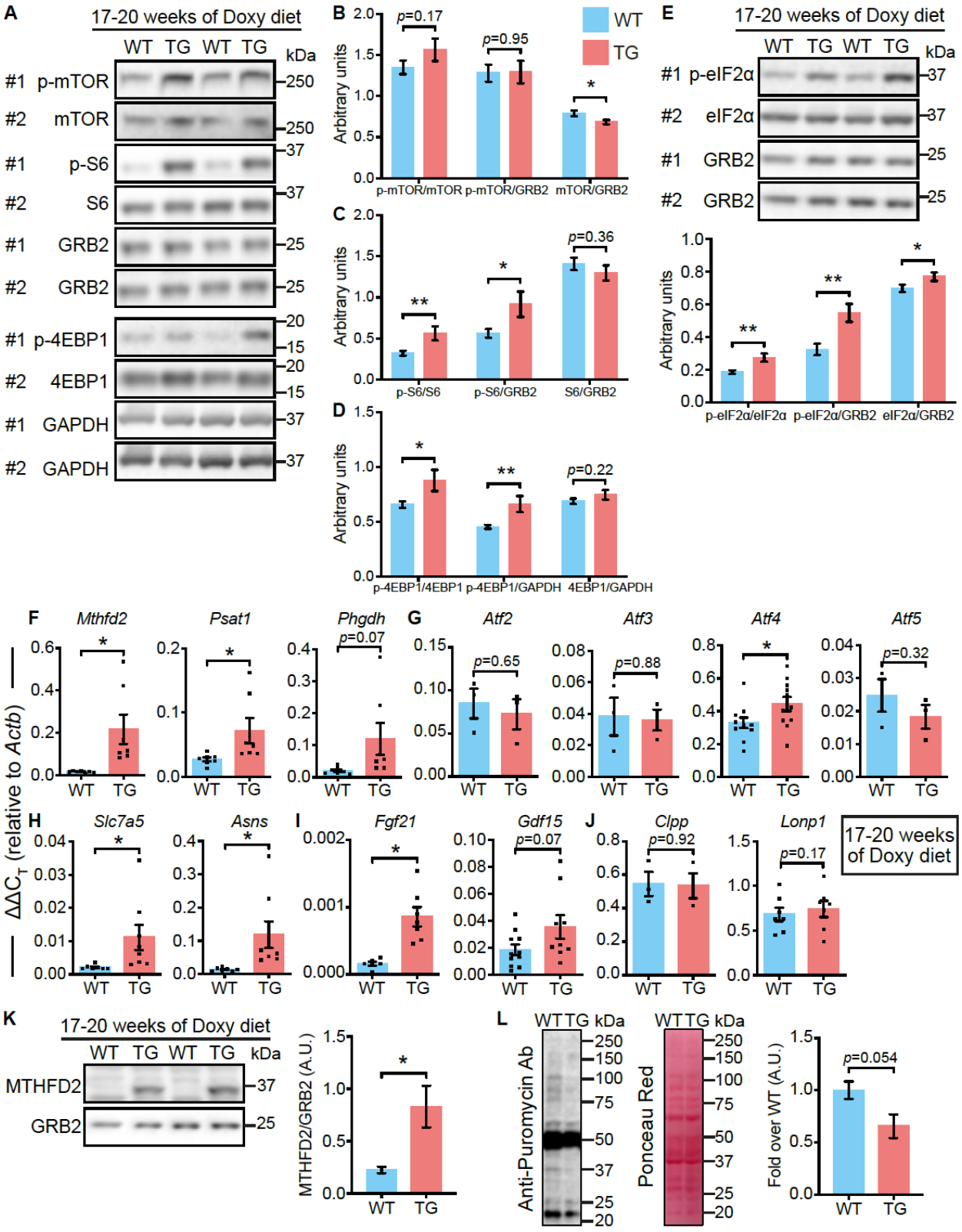
A
17-20 weeks of Doxy diet
WT TG WT TG
kDa
#1 p-mTOR
#2 mTOR
#1 p-S6
#2 S6
#1 GRB2
#2 GRB2
#1 p-4EBP1
#2 4EBP1
#1 GAPDH
#2 GAPDH
B
WT
TG
Arbitrary units
p=0.17
p=0.95
p-mTOR/mTOR
p-mTOR/GRB2
mTOR/GRB2
C
p=0.36
p-S6/S6
p-S6/GRB2
S6/GRB2
D
p=0.22
p-4EBP1/4EBP1
p-4EBP1/GAPDH
4EBP1/GAPDH
E
17-20 weeks of Doxy diet
#1 p-eIF2α
#2 eIF2α
#1 GRB2
#2 GRB2
p-eIF2α/eIF2α
p-eIF2α/GRB2
eIF2α/GRB2
F
Mthfd2
Psat1
Phgdh
p=0.07
G
Atf2
p=0.65
Atf3
p=0.88
Atf4
Atf5
p=0.32
ΔΔC_T (relative to Actb)
H
Slc7a5
Asns
I
Fgf21
Gdf15
p=0.07
J
Clpp
p=0.92
Lonp1
p=0.17
17-20 weeks of Doxy diet
K
17-20 weeks of Doxy diet
MTHFD2
GRB2
MTHFD2/GRB2 (A.U.)
L
Anti-Puromycin Ab
Ponceau Red
Fold over WT (A.U.)
p=0.054

Figure 4: FXN depletion induces an integrated stress response in TG hearts. (A) Representative immunoblots of p-mTOR (Ser2448), mTOR, p-S6 (Ser235/236), S6 p-4EBP1 (Thr70), 4EBP1, GRB2 and GAPDH from heart lysates of WT and TG mice (17-20 weeks of Doxy feeding), with quantification in **(B), (C) and (D)** (n=15 WT and 11 TG; **p*<0.05, ***p*<0.01). **(E)** Representative immunoblot of p-eIF2α(Ser52), eIF2α and GRB2 from heart lysates of WT and TG mice (17-20 weeks of Doxy diet). Averaged p-eIF2α/eIF2α, p-eIF2α/GRB2 and eIF2α/GRB2 values (*lower*) (n=13 WT and 15 TG, **p*<0.05, ***p*<0.01). **(F)** Transcripts values ($\Delta\Delta C_T$) of *Mthfd2*, *Psat1*, *Phgdh* (n=7/genotype, **p*<0.05); **(G)** *Atf2*, *Atf3*, *Atf5* (n=3/genotype), and *Atf4* (n=12/genotype, **p*<0.05); **(H)** *Slc7a5*, *Asns* (n=6-7/genotype, **p*<0.05); **(I)** *Fgf21*, *Gdf15* (n=7/genotype, **p*<0.05, ***p*<0.01).; **(J)** *Clpp* and *Lonp1* (n=3 and 8/genotype, respectively). All trancripts were normalized to *Actb* (β-actin). **(K)** Representative immunoblot of MTHFD2 and GRB2. GRB2 was used as a loading control. *Right:* Quantification of MTHFD2/GRB2 values (n=6 WT/TG). (**L**) Global protein translation revealed by immunoblot of puromycin detection, using SUnSET technique. Ponceau Red staining was used to estimate the protein loading (*Middle*). *Right*: Quantification of puromycin signal (n=4 per genotype). In all cases, values represent the mean ± s.e.m. Statistical comparison was by unpaired t-test.

Figure 5

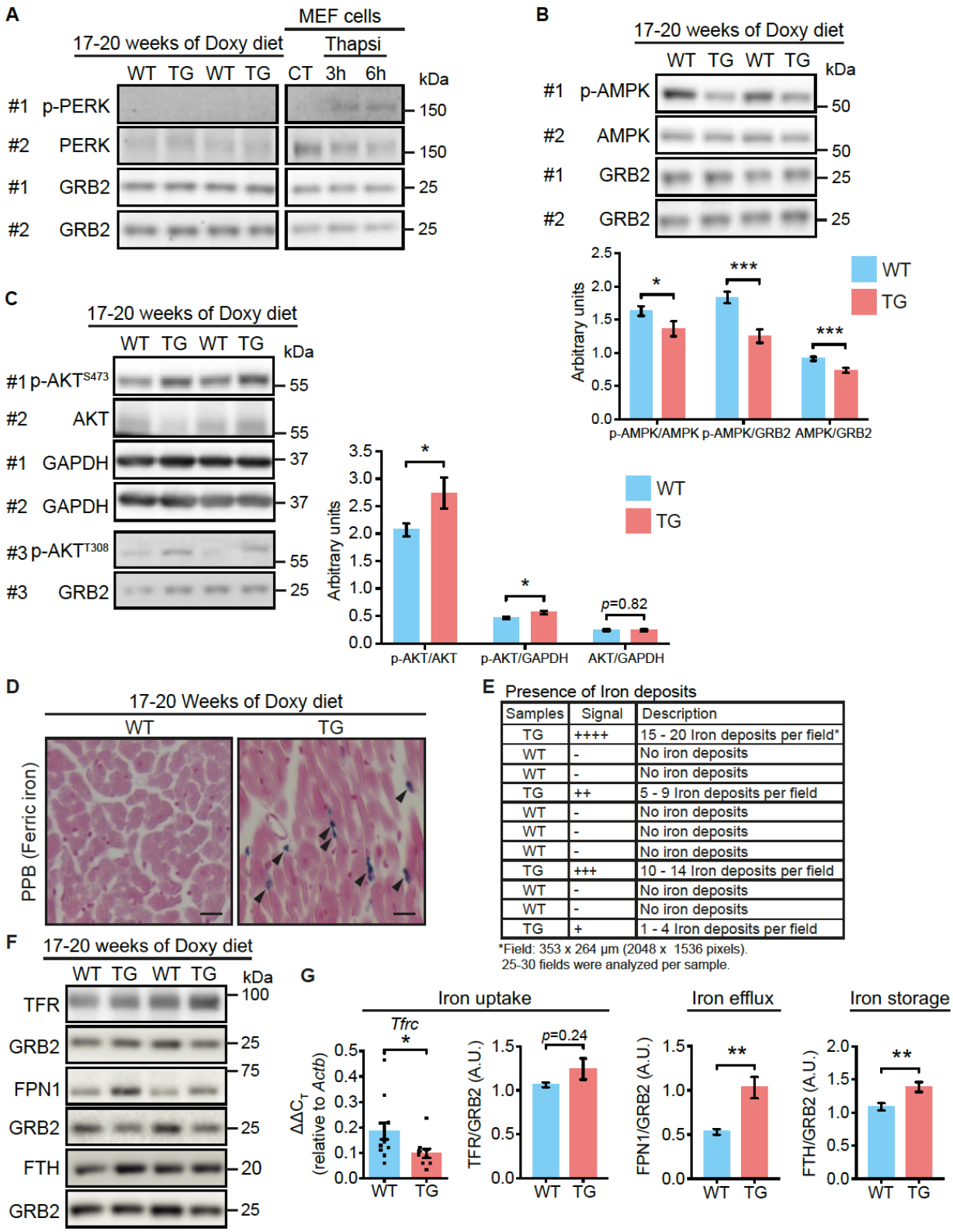
A
MEF cells
17-20 weeks of Doxy diet
Thapsi
WT TG WT TG CT 3h 6h
kDa
#1 p-PERK 150
#2 PERK 150
#1 GRB2 25
#2 GRB2 25
B
17-20 weeks of Doxy diet
WT TG WT TG
kDa
#1 p-AMPK 50
#2 AMPK 50
#1 GRB2 25
#2 GRB2 25
Arbitrary units
p-AMPK/AMPK p-AMPK/GRB2 AMPK/GRB2
WT
TG
C
17-20 weeks of Doxy diet
WT TG WT TG
kDa
#1 p-AKT S473 55
#2 AKT 55
#1 GAPDH 37
#2 GAPDH 37
#3 p-AKT T308 55
#3 GRB2 25
Arbitrary units
p-AKT/AKT p-AKT/GAPDH AKT/GAPDH
p=0.82
WT
TG
D
17-20 Weeks of Doxy diet
WT TG
PPB (Ferric iron)
E
Presence of Iron deposits
Samples | Signal | Description
TG | ++++ | 15 - 20 Iron deposits per field*
WT | - | No iron deposits
WT | - | No iron deposits
TG | ++ | 5 - 9 Iron deposits per field
WT | - | No iron deposits
WT | - | No iron deposits
WT | - | No iron deposits
TG | +++ | 10 - 14 Iron deposits per field
WT | - | No iron deposits
WT | - | No iron deposits
TG | + | 1 - 4 Iron deposits per field
*Field: 353 x 264 µm (2048 x 1536 pixels).
25-30 fields were analyzed per sample.
F
17-20 weeks of Doxy diet
WT TG WT TG
kDa
TFR 100
GRB2 25
FPN1 75
GRB2 25
FTH 20
GRB2 25
G
Iron uptake
Iron efflux
Iron storage
Tfrc
ΔΔC_T (relative to Actb)
TFR/GRB2 (A.U.)
p=0.24
FPN1/GRB2 (A.U.)
FTH/GRB2 (A.U.)
WT TG

Figure 5: Investigation into possible upstream regulators of eIF2α and mTORC1. (A) To evaluate possible ER stress, representative immunoblots of p-PERK (Thr980), PERK and GRB2 from heart lysates of WT and TG mice (17-20 weeks of Doxy diet) (n=13 WT and 15 TG). MEF cells treated with thapsigargin (1 μM) to induce ER stress were used as positive control for PERK activation. **(B)** Representative immunoblots of p-AMPK (Thr302), AMPK and GRB2. *Lower panel*: Averaged p-AMPK/AMPK, p-AMPK/GRB2 and AMPK/GRB2 values (n=15 WT/11 TG, *p<0.05, ***p<0.001). **(C)** Representative immunoblots of p-AKT (Ser473), p-AKT (Thr308), AKT, GRB2 and GAPDH. *Right panel*: Averaged p-AKT(Ser473)/AKT, p-AKT (Ser473)/GAPDH and AKT/GAPDH values (n=15 WT and 12 TG, *p<0.05, ***p<0.001). For p-AKT/Thr308, GRB2 (n=4 WT and 5 TG). **(D)** Cross-sections from heart (WT and TG from 17-20 weeks of Doxy feeding) stained with Pearls' Prussian Blue (PPB) to reveal iron deposition (n=7 WT and 4 TG). **(E)** Qualitative score of PPB-stained sections to evaluate abundance of iron deposits. **(F)** Representative immunoblots of TFR, FPN1 and FTH and Grb2. **(G)** Relative mRNA levels ($\Delta\Delta C_T$ values) of *Tfrc*, normalized to *Actb* (β-actin) (n=12 WT/10 TG, **p<0.01). Protein levels of TFR, FPN1 and FTH are displayed in bar graphs (n=4-7 WT, 5-6 TG, **p<0.01). All values: mean ± s.e.m. Statistical comparison was by unpaired t-test.

Supplemental Figure 1

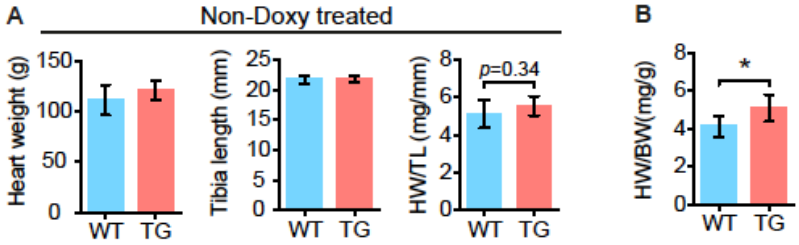

Figure S1: Non-doxy treated mice cardiac parameters and HW/BW in doxy-treated mice. Related to Figure 1. (A) Heart weight (HW), tibia length (TL), and tibia length to heart weight ratio (HW/TL) of non-doxy treated mice (n=9 WT and 4 TG). **(B)** Heart weight to body weight ratio (HW/BW) after 17-20 weeks of Doxy feeding (n=7/genotype, *p<0.05). All values: mean ± s.e.m. Statistical analysis was by unpaired t-test.

Supplemental Figure 2

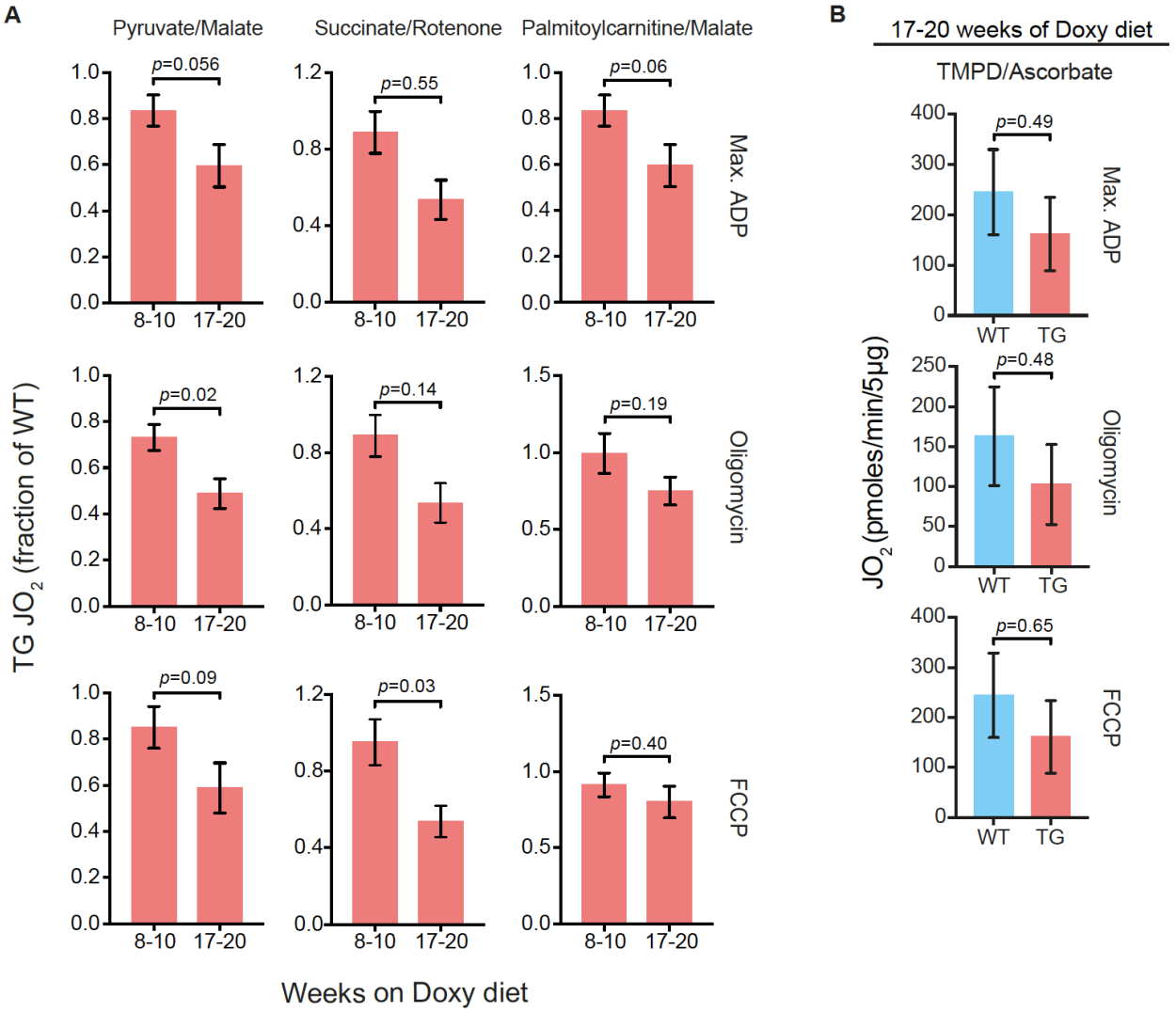

Figure S2: Differences over time of substrate oxidation. Related to Figure 2. (A) Oxygen consumption rate (JO_2) measurements from isolated heart mitochondria from WT and TG mice (8-10 and 17-20 of Doxy diet), using pyruvate/malate, succinate/rotenone and palmitoyl-L-carnitine/malate, as substrates (same conditions as Figure 2B). Each TG JO_2 value was expressed as a fraction of corresponding WT JO_2 value. Sample sizes: 8-10 weeks Doxy: n=7/genotype; 17-20 weeks Doxy: n=5/genotype; *p<0.05, **p<0.01, using one-way ANOVA analysis. **(B)** TMPD/ascorbate JO_2 measurements. Oxygen consumption rate (JO_2) measurements from isolated heart mitochondria from WT and TG mice from 17-20 of Doxy diet, using TMPD/ascorbate (1 mM/2 mM) (n=4/genotype). All values are mean ± s.e.m. Statistical analysis was by unpaired t-test.

Supplemental Figure 3

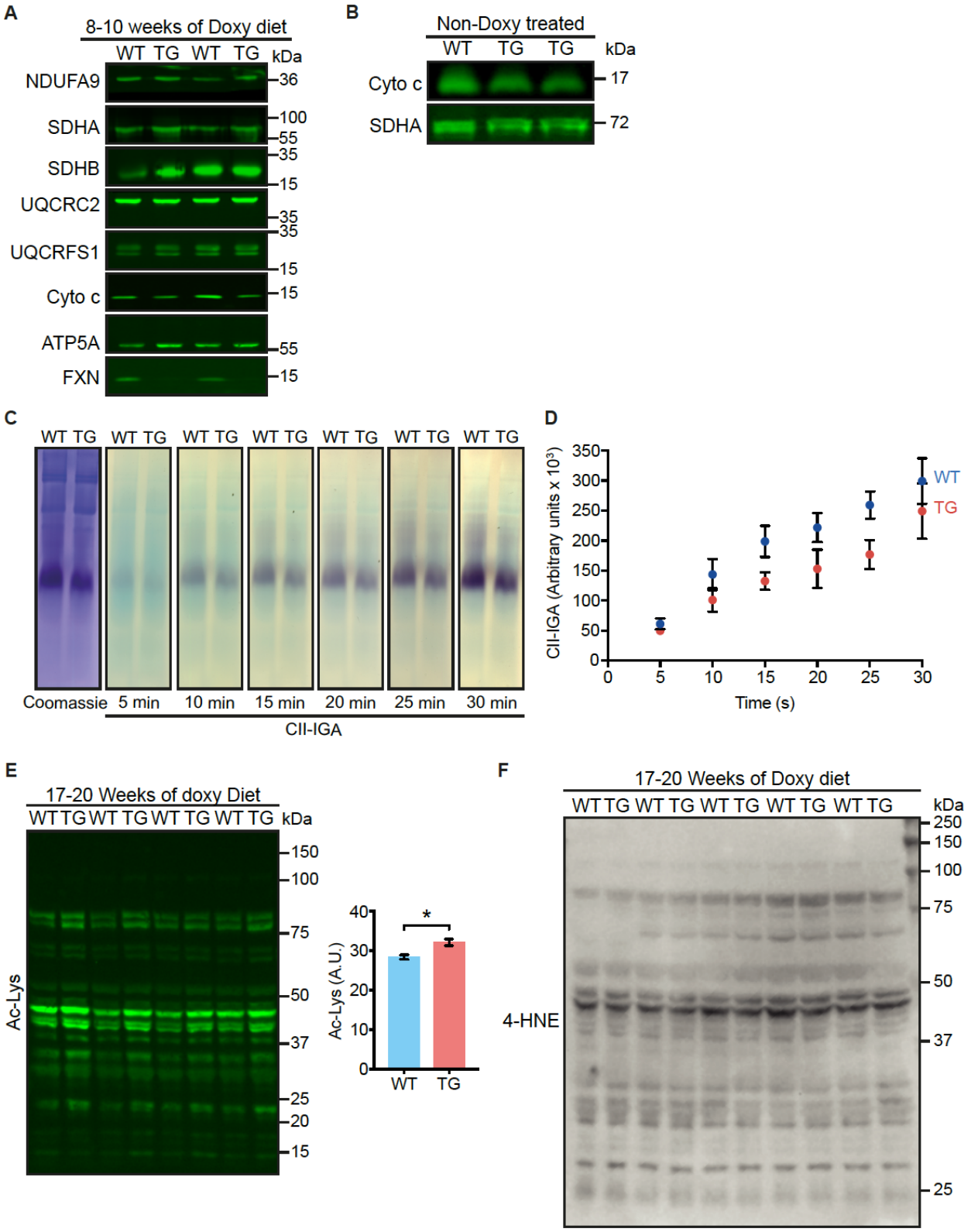

Figure S3. Levels of electron transport chain subunits, supercomplexes and in-gel activity. Related to Figure 3. (A) Representative immunoblots electron transport chain subunits from isolated heart mitochondria from WT and TG mice (8-10 weeks of Doxy diet). **(B)** Immunoblot of Cytochrome c (Cyto c) and SDHA in from isolated mitochondria from non-doxy treated mice (n=1WT and 2TG). (**C)** Complex II (CII)-IGA (from 5-30 min of reaction) and Coomassie staining representative images; **(D)** Quantification of CII-IGA values for each time point (n=5/genotype). **(E)** Immunoblot of acetylated lysine (Ac-Lys) residues from isolated heart mitochondria of WT and TG mice (17-20 weeks of Doxy diet) (n=4WT/4TG, *p<0.05). **(F)** Immunoblot of 4-hydro-nonenal (4-HNE) modification from isolated heart mitochondria of WT and TG mice at 17-20 weeks of doxy-diet (n=5WT/TG). All values represent mean ± s.e.m. Statistical analysis was done by unpaired t-test.

Supplemental Figure 4

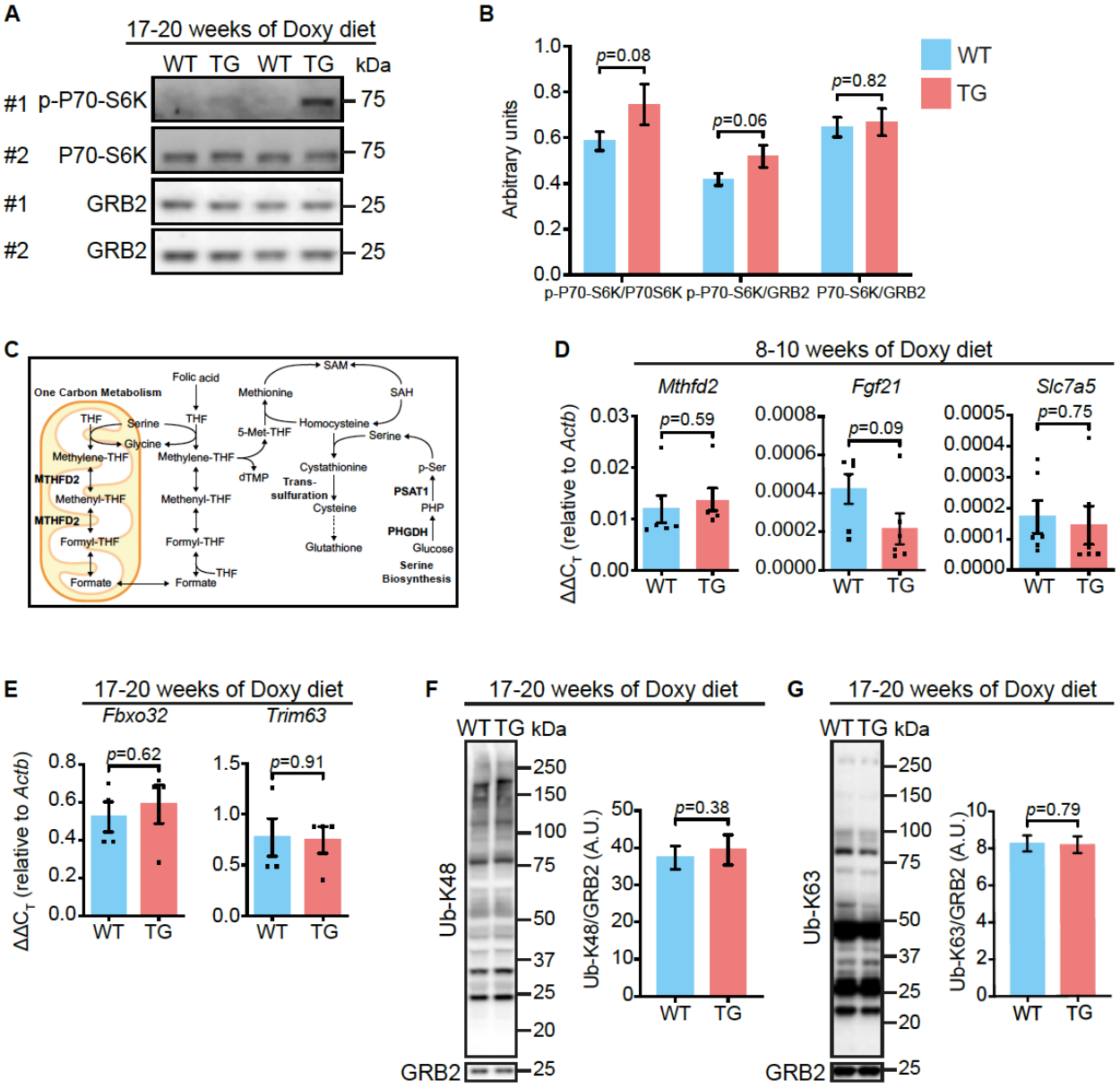

Figure S4. P70S6K phosphorylation levels, stress response transcript levels and evaluation of protein degradation. Related to Figure 4. (A) Representative immunoblot of p-P70-S6K (Thr389), P70-S6K and GRB2 from heart lysates of WT and TG mice (17-20 weeks of Doxy diet). **(B)** Averaged p-P70-S6K/P70-S6K, p-P70-S6K/GRB2 and P70-S6K/GRB2 values (*lower*) (n=15 WT and 12 TG). **(C)** Schematic representation of one-carbon metabolism and serine biosynthesis pathways altered during integrated stress response. **(D)** *Actb* (β-actin)-normalized transcripts values ($\Delta\Delta C_T$) of *Mthfd2*, *Fgf21* and *Slc7a5* from WT and TG hearts from 8-10 weeks Doxy-fed mice (n=4 mice/genotype). **(E)** mRNA levels of *Fbxo1* (Atrogin1) and *Trim63* (MuRF1), involved in protein degradation. Each transcript value ($\Delta\Delta C_T$ value) was normalized to *Actb* (β-actin) (n=4/genotype). **(F)** Representative immunoblot of poly-ubiquitinated proteins with specific Ub-K48 linkage and **(G)** Ub-K63 linkage. GRB2 was used as a loading control. *Right*: Quantification of Ub-K48/GRB2 and Ub-K63/GRB2, respectively (n= 6 WT and 4 TG mice). In all cases, values represent the mean ± s.e.m. Statistical comparison was by unpaired t-test. All values: mean ± s.e.m

Supplemental Figure 5

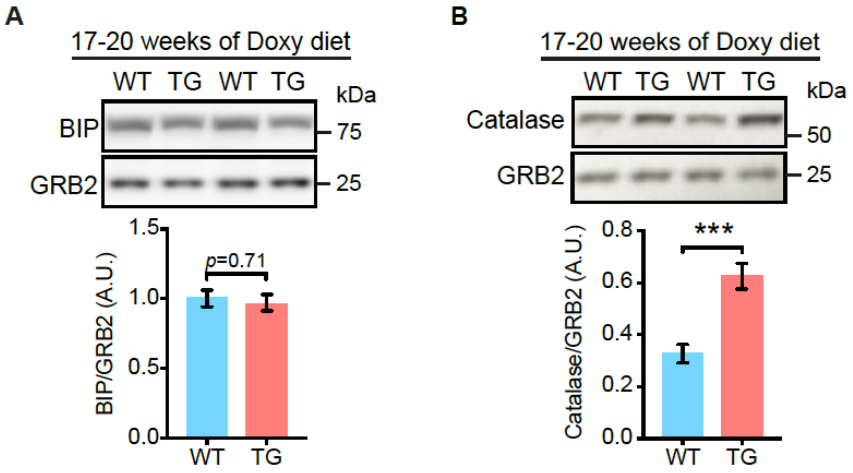

Figure S5. ER stress marker BIP and catalase protein levels. Related to Figure 5. (A) Representative immunoblot of BIP and GRB2 from heart lysates of WT and TG mice (17-20 weeks of Doxy diet). *Lower*: Averaged BIP/GRB2 values (n=13WT and 15TG mice). **(B)** Representative immunoblot of catalase and GRB2 from heart lysates of WT and TG mice (17-20 weeks of Doxy diet). *Lower*: Averaged catalase/GRB2 values (n=9WT and 10TG mice, (***$p<0.001$).

Supplemental Figure 6

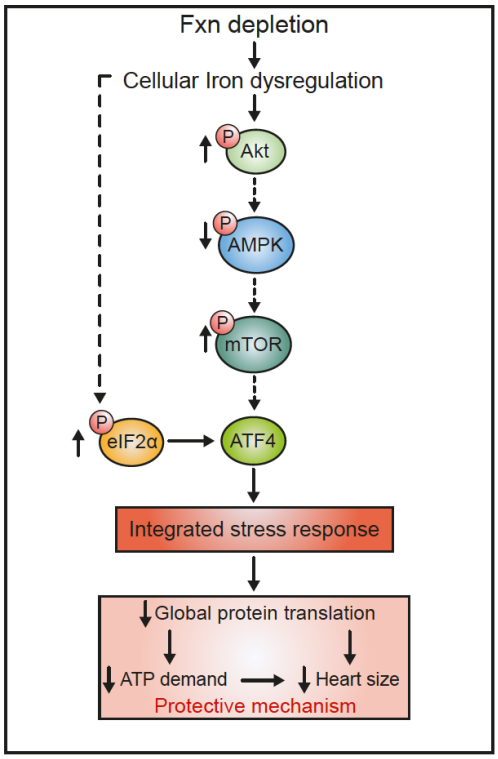

Figure S6. Summary of changes in nutrient and stress signaling in the heart of mice with adult-onset FXN depletion for ~20 weeks, and hypothesized causal connections (dashed lines).

Supplemental Figure 7

Table I: Depletion of Fe-S cluster biogenesis pathway components: Differential impact on Fe-S cluster proteins		
Fe-S cluster pathway component	Biological Source	Enzyme activity (from most to least impaired)
1 ↓Fxn	Human FA patients (skm)	Aconitase = SDH > C-I = C-III
↓Fxn	Human FA patients (heart)	Aconitase = SDH > C-I > C-III
2 ↓NFU1 (siRNA)	HeLa cells	PDH > SDH > mito Aconitase
↓ISCU (siRNA)	HeLa cells	SDH > PDH = mito Aconitase
↓NFU1 (gly208lys mutation)	Yeast	PDH > SDH > mito Aconitase
↓NFU1 (C545+5G>A)	Yeast	PDH = TCA cycle > SDH >> C-I
3 ↓ISD11	Human mutation (skm)	C-I = C-II = C-III (all ≤ 10% normal)
↓ISD11	Human mutation (liver)	C-I = C-II > C-III (normal)
4 $ISCU^{D71A}$	HEK cells	mito Aconitase > SDH > C-I
$ISCU^{C69S}$	HEK cells	mito Aconitase > SDH > C-I

References:
1) Rötig et al, 1997, Nat Med.;
2) Navarro-Sastre et al, Am J Human Genet, 2011;
3) Lim SC et al, Hum Mol Genet, 2013;
4) Crooks DR et al, J Biol Chem, 2018.

Figure S7. Table summarizing literature results on the effects of depletion of Fe-S cluster biogenesis components on the activity of Fe-S cluster-containing proteins.